Form-finding and metaheuristic multiobjective optimization methodology for sustainable gridshells with reduced construction complexity and waste

Automation in Construction 177 (2025) 106315

Contents lists available at ScienceDirect

Automation in Construction

journal homepage: www.elsevier.com/locate/autcon

Form-finding and metaheuristic multiobjective optimization methodology for sustainable gridshells with reduced construction complexity and waste

Jonathan Melchiorre [a,*], Amedeo Manuello Bertetto [a], Sigrid Adriaenssens [b], Giuseppe Carlo Marano [a,c]

[a] Politecnico di Torino, DISEG, Department of Structural, Geotechnical and Building Engineering, Corso Duca Degli Abruzzi, 24, Turin, 10129, Italy
[b] Princeton University, Department of Civil and Environmental Engineering, E208 Engineering Quadrangle, Princeton, NJ, 08544, USA
[c] Henan University of Technology, School of Civil Engineering and Architecture, 100 Lianhua St, Zhongyuan District, Zhengzhou, Henan, 450001, China

ARTICLE INFO

Keywords:
Gridshells
Waste reduction
Form-finding
Multiobjective optimization
Multi-body rope approach
Genetic algorithm
Dynamic equilibrium methods

ABSTRACT

The construction industry is one of the sectors with the highest environmental impact, yet it constitutes an important part of the global economy. Therefore, minor improvements in this sector can lead to substantial global benefits. Structural optimization protocols offer promising solutions to this challenge, especially for gridshell structures. Given the complexities involved in constructing gridshells, optimization techniques can play a crucial role in enhancing design by reducing material usage, and improving construction efficiency. This paper presents a methodology for the optimization of gridshell structures using the NSGA II optimization algorithm, combined with the improved Multi-body Rope Approach (i-MRA) form-finding method. The primary objective of this methodology is to minimize the variety of structural elements, reduce material consumption, decrease production waste, and ensure adherence to structural verification standards. This methodology provides an efficient approach for the conceptual design of gridshell structures.

1. Introduction

The construction industry (CI) is a major contributor to environmental impact, accounting for a significant portion of the human ecological footprint. It is responsible for around 30% of global greenhouse gas emissions [1], consumes nearly half of the world raw materials, and utilizes 40% of global energy [2]. Additionally, CI contributes to 50% of landfill waste globally [3] and is expected to see a doubling of global building floor area by 2050 due to population growth and increasing affluence in emerging economies [4]. These environmental challenges represent risks to ecosystems, and public health, and exacerbate climate change. Despite these concerns, the construction industry remains a key driver of the global economy, contributing 10% to the world Gross Domestic Product (GDP), equivalent to 7.5 trillion USD. In the European Union (EU), CI supports approximately 18 million direct jobs and contributes 9% to the GDP [5]. Considering the importance of the CI in both environmental and economic terms, even minor improvements in this sector have the potential to have a profound impact on a global scale.

The integration of structural optimization methods into standard practices becomes crucial in this context. The prospective implications of structural optimization in the construction industry become much more obvious as projections are extended to 2050. Estimates [4] suggest that by applying structural optimization techniques, a decrease of over 95 million metric tons of concrete and more than 3000 million kilogrammes of steel can be achieved, leading to significant energy savings of more than 100 trillion British Thermal Unit (BTU) per year, and an annual decrease in greenhouse gas (GHG) emissions by more than 10 million metric tons of CO_2 equivalent [4].

Recently, there has been a notable expansion in the quantity and quality of structural optimization studies have advanced the field. The majority of these studies have three main objectives: (1) minimizing economic costs, (2) enhancing structural performance [6] and (3) reducing environmental impact of structures. For gridshells, optimization objectives diverge from objectives formulated for more conventional structures. Gridshell structures are characterized more by construction complexity than by inefficient material utilization [7]. The construction challenge has impeded their widespread adoption. For this reason, several studies have explored the application of optimization algorithms to address the associated technological challenges. For instance, these studies have concentrated on optimizing structural nodes [8–10], optimal topologies for structural elements [11–13], or the best panelling patterns [14,15]. Additionally, there has been research into innovative construction methods [16,17].

* Corresponding author.
E-mail address: jonathan.melchiorre@polito.it (J. Melchiorre).

https://doi.org/10.1016/j.autcon.2025.106315
Received 21 December 2024; Received in revised form 28 May 2025; Accepted 29 May 2025
Available online 20 June 2025

Several approaches have been proposed to address geometric constraints in modelling problems. For example, [18] propose a differential–geometric approach that minimizes total absolute curvature and aligns principal stress directions, generating optimal structures and minimizing material usage. More recently, [19] introduced the Guided Projection Algorithm (GPA), which is an iterative optimization technique that combines guided projections with a regularization strategy. The GPA can be considered a regularized Newton method [20] with an appropriate damping mechanism. Conceptually, it is similar to the Levenberg–Marquardt algorithm [21] and is designed to solve nonlinear constraint equations. The method is based on the introduction of auxiliary variables, which are used to reformulate complex constraints such that they become at most quadratic. It involves the iterative projection of the solution onto the constraint manifold, with the use of regularization to maintain stability. This guided, regularized optimization allows the solver to converge robustly and with high precision, often satisfying constraints to machine accuracy.

From a structural perspective, gridshells exemplify the mechanical behaviour of shells, integrating the smooth curves of shell structures with the simplicity and versatility of straight beam elements. Despite being composed of linear structural elements, the spatial configuration of these elements enables gridshells to exhibit a spatial behaviour typically associated with shell structures. Their curved shape offers an optimal morphology for accommodating various load patterns and stress paths, resulting in optimal material usage and high structural efficiency. The curved grid structure offers both structural and aesthetic benefits [22], as it allows for the construction of large-span structures without the need intermediate supports like columns. The gridshell concept exploits the capacity of shell structures to resist loading through membrane-type actions, which are primarily associated with plane stress. This design approach ensures that the structural elements of the gridshell primarily experience compressive or tensile stresses rather than bending stresses [23]. The structural efficiency of gridshell structures is significantly influenced by their morphological definition.

Over the years, a plethora of methodologies have been devised for form-finding shells and gridshells. These methods are the Thrust Network Analysis (TNA) [24], Force Density Method (FDM) [25], Particle-Spring System [26], Dynamic Relaxation (DR) [27,28], Multibody Rope Approach (MRA) [29], and others [30–33]. These methodologies during the conceptual design phase enable the definition of structurally form found shapes. A traditional design approach for gridshells involves form-finding methods to define an efficient structural form for a specific set of loads (usually self-weight) and boundary equations. The optimization techniques are employed to enhance the complex construction process to address the technological challenges inherent in this structural type [34]. In this context, some studies investigated the possibility of combining form-finding and optimization techniques [35–37]. The main challenges is to define a structural model that is structurally and constructively optimized. The optimization of structural element production and the management of construction stages introduce additional challenges in form-finding and optimization because they demand a balance between idealized designs and practical constraints. Structural forms optimized for performance often feature complex geometries that require advanced manufacturing methods, increasing the difficulty of achieving precision while minimizing waste. Integrating these considerations ensures that designs are not only structurally efficient but also feasible to fabricate and assemble aligning with real-world production and construction requirements. A two-phase methodology was proposed for the preliminary structural design of grid shell structures which combines form-finding through the Dynamic Relaxation (DR) method with optimization through the Genetic Algorithm (GA) [38]. The objectives were the minimization of material usage and the enhancement of structural performance. In another study [39] was presented an optimization approach combining form-finding (FF), sizing-optimization (SO), and topological-optimization (TO) strategies in a multilevel process. Another optimization procedure [40] optimized the shape of an elastic gridshell for a given grid. The forces applied to erect the gridshell are chosen as design variables of the optimization problem. The method of moving asymptotes was used to solve the problem, while the implicit DR was employed to define the shape.

In this paper a new methodology is presented for the preliminary design of gridshell structures. It combines a free-form base gridshell form-finding method [41] with a multi-objective metaheuristic optimization algorithm [42]. In particular, the methodology utilizes the improved Multibody Rope Approach (i-MRA) [43] for structural shape definition. This method builds upon the classical Multibody Rope Approach [29]. To enhance accessibility and practical application of the i-MRA form-finding method, a software component has been developed to integrate it within the parametric design software Grasshopper, which operates in the Rhinoceros3D environment [44]. The method involves numerically modelling a system of nodal masses connected by inextensible ropes. As the length of the ropes constituting the system varies, different structural shapes can be obtained, each of which is funicular with respect to the acting loads. The lengths of the ropes can significantly impact the shape and degree of sag of the structures defined. These lengths represent the parameters of the form-finding method, and their selection depends on various factors specific to the structural design. In this paper an automatic method is proposed for obtaining these parameters by defining a structural optimization problem. In particular, the idea is to define the combination of parameters that will minimize the amount of structural material for the gridshell's construction and at the same time minimize the types of structural elements required to build it. Two objective functions are defined to minimize the costs related both to the material usage and to the easiness of construction. For this purpose, a state-of-art multiobjective optimization algorithm, the Non-Dominated Sorting Genetic Algorithm (NSGA II), is employed to identify the optimized solutions set [45]. The optimization problem was constrained to ensure that the resulting structural configurations passed specific structural criteria, including uniaxial load, maximum global deformation, and local buckling of the structural elements [46].

Finally, production waste was considered. In general, structural optimization typically focuses on minimizing the net material required for construction. In reality, the solution with the lowest net material usage may not necessarily have the lowest gross material usage [47]. For instance, in the case of steel gridshells, structural elements are often produced by cutting steel billets of constant length. However, gridshells may require elements of varying lengths, necessitating an efficient cutting pattern to minimize waste. This problem is known as the Cutting Stock Problem (CSP) and has been extensively studied [48]. In this study, a solution based on linear programming algorithms is chosen to address this issue [49]. The CSP solution enables the definition of a cutting pattern with minimal waste and determines the minimum number of billets needed for producing structural elements. This approach allows for the computation of material consumption inclusive of waste, ensuring that production waste is also considered in the optimization problem [50]. The entire process and analysis are performed using custom code developed in MATLAB [51], which provides a versatile computational framework for optimization and analysis.

The proposed approach aims to rationalize the construction process, reduce costs and promote sustainable practices in gridshell design. Three case studies are presented to demonstrate the effectiveness of the approach. The first case study focuses on a square gridshell subjected to self-weight and various nodal forces. Optimization results are presented in terms of the number of different structural element types and the quantity of material used. The second case study investigates the optimization of a regular yet more complex gridshell. It features a central rectangular space with a square opening, seamlessly connected to four smaller rectangular zones extending from its corners. The third case study comprises a free-form base gridshell, illustrating the application

of the methodology to a non-standard geometry. This case study serves to illustrate the versatility and effectiveness of the proposed approach in optimizing gridshell structures for a variety of design scenarios. The results are compared for different loading conditions, with regard to the number of different element typologies, net material consumption, and waste.

The paper is structured as follows: Section 2 provides an overview of the form-finding methodology. Section 3 presents the definition of the structural optimization problem including the formulation of the multi-objective optimizer. Section 3.4 describes the multiobjective optimization algorithm used in the study. In Section 4, three case studies are analysed to demonstrate the effectiveness and the applicability of the proposed methodology. Section 5 concludes the paper and discusses potential future developments.

2. Form-finding with improved multibody rope approach

In this section outlines the form-finding methods employed during the optimization process is defined. Initially, the Multi-Body Rope Approach (MRA) is presented, followed by an account of the modifications that led to its improved version, the i-MRA. This method defines structural shapes that are both easy to construct and optimized to resist applied loads effectively.

2.1. Multi-body rope approach

The Multibody Rope Approach (MRA) [29] is a technique employed for the form-finding of free-form base gridshell structures. This method involves numerically solving a system of nodal masses connected by loose ropes.

According to the taxonomy of form-finding techniques proposed in [52], the Multibody Rope Approach (MRA) is classified as a *Dynamic Equilibrium Method*. This category includes methods that determine the shape of a structure by solving dynamic equilibrium equations through a time-dependent simulation process that converges to a static configuration. Dynamic Relaxation (DR) [27] is considered the first and most widely adopted approach in this category. DR computes equilibrium shapes by integrating the equations of motion using explicit time-stepping and artificial damping. This allows the system to dissipate kinetic energy progressively until a stable geometric configuration is achieved. The MRA preserves the underlying dynamic equilibrium strategy of *Dynamic Equilibrium Methods*, but introduces a distinct force application scheme and utilizes inextensible rope elements specifically designed to maximize structural efficiency and constructability.

The Multibody Rope Approach (MRA) employs the mass of the nodes and an additional system of nodal loads to define the funicular structural form with respect to the assigned loads. In MRA, equilibrium forces are imposed on each node in accordance with Eq. (1).

$$\vec{R}_i = \vec{p}_i + \sum_{j=1}^{n_i} \vec{F}_{rope,ji} + \vec{F}_i^{I} + \vec{F}_i^{II} = 0 \tag{1}$$

The resultant of the forces $\vec{R}_i$ is the sum of the external loads p_i, the forces exerted by the ropes connected to the node $\vec{F}_{rope,ji}$, and the inertial $\vec{F}_i^{II} = \ddot{\vec{u}}_i = (\ddot{x}_i, \ddot{y}_i, \ddot{z}_i)$ and damping forces $\vec{F}_i^{I} = \dot{\vec{u}}_i = (\dot{x}_i, \dot{y}_i, \dot{z}_i)$ due to the node mass.

The force exerted by the ropes is modelled as a bi-linear acting force (Eq. (2)) as function of the distance between two connected nodes l.

$$\begin{cases} F_{rope} = 0 & \text{if} \quad l < l_{rope} \\ F_{rope} = k(l - l_{rope}) & \text{if} \quad l \geq l_{rope} \end{cases} \tag{2}$$

In Eq. (2), the forces are expressed in terms of their magnitudes.

It is important to note that ropes do not exert compressive reactions (when $l < l_{rope}$), but rather provide an elastic reaction during tensile phases ($l \geq l_{rope}$), which is proportional to the elongation of the rope relative to its resting length ($l - l_{rope}$). The proportionality coefficient, k, represents the elastic coefficient of the ropes. In common usage of MRA, k is chosen to be very high in order to simulate effectively the behaviour of inextensible ropes.

The funicular form is that corresponding to the configuration in which the resultant of the forces $\vec{R}_i$ acting on all nodal masses is equal to zero. By explicating the forces of inertia and damping, it is possible to rewrite the equation of equilibrium in the form:

$$\ddot{\vec{u}} + 2\omega_n\zeta\dot{\vec{u}} = \frac{1}{m}\left\{\vec{p}_i + \sum_{j=1}^{n_i} \vec{F}_{rope,ji}\right\} \tag{3}$$

In Eq. (3), the symbols $\ddot{\vec{u}}$, $\dot{\vec{u}}$, and ω_n represent, respectively, the nodal accelerations, the velocities of the nodes, and the natural frequency of the dynamical system. The symbol ζ represents the critical damping.

$$\omega_n = \sqrt{\frac{k}{m}} \tag{4}$$

$$\zeta = \frac{c}{2\omega_n m} \tag{5}$$

In Eqs. (4) and (5), k is the stiffness, m is the mass, and c is the damping coefficient of the system. The solution to the equilibrium equation can be obtained by combining the solution of the associated homogeneous equation with the particular solution. The solution is thus represented by Eq. (6) where $\vec{u}(t)$ represents the position of the nodes at the time t.

$$\vec{u}(t) = \vec{C}_1 e^{-2\omega_n\zeta t} + \vec{C}_2 + \frac{\vec{C}_3}{2\omega_n\zeta}t \tag{6}$$

The coefficients in the complete solution are functions of the dynamic parameters of the system, the forces applied to the nodes, and the initial conditions (position and velocity) of the nodal masses.

$$\vec{C}_1 = -\frac{2\omega_n\zeta\dot{\vec{u}}_{(t-\Delta t)} - \vec{C}_3}{(2\omega_n\zeta)^2} \tag{7}$$

$$\vec{C}_2 = -\frac{(2\omega_n\zeta)^2\vec{u}_{(t-\Delta t)} + 2\omega_n\zeta\ddot{\vec{u}}_{(t-\Delta t)} - \vec{C}_3}{(2\omega_n\zeta)^2} \tag{8}$$

$$\vec{C}_3 = \frac{1}{m}\left\{\vec{p}_i + \sum_{j=1}^{n_i} \vec{F}_{rope,ji}\right\} \tag{9}$$

As the forces exerted by the ropes vary depending on the reciprocal position of the nodes, the system must be solved iteratively. In each time-step, the position, velocity and accelerations of the nodes calculated in the previous time-step are taken as initial conditions.

Upon achieving equilibrium configuration of the hanging net, the majority of the initially slack ropes are now tensioned. Since these ropes lack bending stiffness, they are subjected exclusively to axial tensile stress. By inverting this equilibrium configuration and substituting the ropes with beam-type structural elements, a funicular structure can be obtained.

It is important to clarify the concept of 'funicular configuration' as used in this work. A funicular structure traditionally refers to a configuration where elements experience only axial forces (either tension or compression) under a specific loading pattern. In the context of the hanging net model obtained with the MRA, the funicular configuration is achieved when the resultant of forces at each node equals zero, with rope elements either in tension or slack (unstressed, tension equal to 0). After form-finding, not all ropes are necessarily tensioned due to geometric redundancy in the system, particularly when a node connects to more than three non-coplanar elements. When the hanging net configuration is inverted and the rope elements are replaced with beam elements to form a gridshell, the formerly tensioned elements will primarily experience compression. The previously slack elements become integral parts of the structural system, and due to the flexural stiffness of the beam elements, all elements will experience some degree of parasitic bending in addition to axial forces. Parasitic bending refers to the secondary bending moments that inevitably develop in gridshell structures composed of beam elements, even when the overall

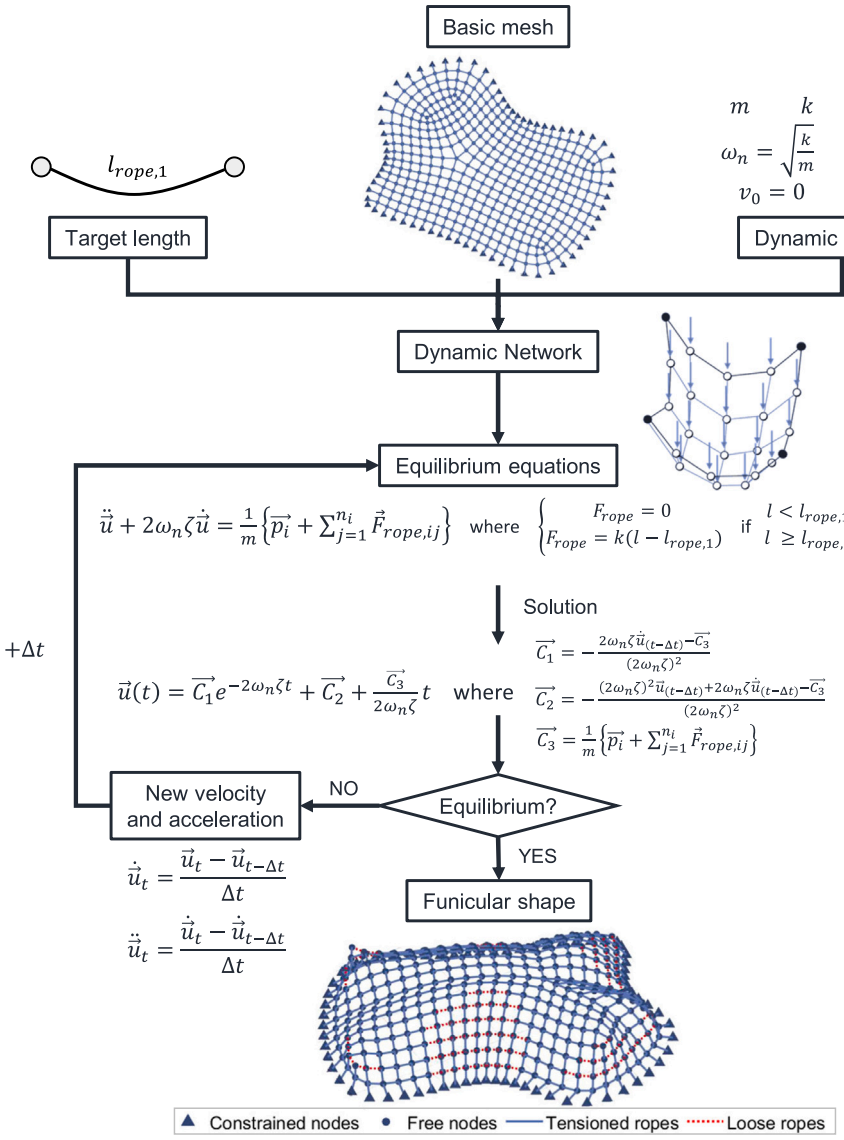

Fig. 1. MRA workflow.

form closely follows a funicular shape. This bending arises from the discrete nature of the grid, boundary conditions, the inherent flexural stiffness of structural elements and the fact that real elements deform, causing the final loaded configuration to deviate slightly from the one calculated through form-finding [36].

Fig. 1 illustrates the process by which the MRA allows the funicular structural form to be defined through the solution of the presented equilibrium equations.

2.2. Improved multi-body rope approach

In Section 2.1 it was shown how the MRA method determines a funicular structural configuration in response to applied loads. This funicular form represents a structurally optimal configuration, as the structural elements are subjected mostly to axial internal loadings.

In this state, most of the ropes connected to each node will be tensioned, although not necessarily all of them. Each node has three spatial degrees of freedom, and each tensioned rope acts as a spatial constraint. When more than three ropes are connected to a single node, an equilibrium configuration can be achieved without all ropes being tensioned. Consequently, the model will contain both taut and slack ropes. Geometrically, the distance between two nodes connected by taut ropes will be equal to the length of the rope l_{rope}. Conversely, for nodes connected by slack ropes, their distance can vary but will be less than l_{rope}.

In the final geometry, structural elements can be categorized into two groups based on their length. Those shorter than l_{rope} are termed *loose elements*, while those with a length equal to l_{rope} are designated as *target elements*.

From a constructional standpoint, the presence of *loose elements* can pose significant challenges. Structural elements represented by these *loose ropes* have varying lengths and complicate both the production of these elements and the assembly of the overall gridshell.

To address this challenge and improve the structural shape from a constructional perspective, an improved version of the MRA, called the improved MRA (i-MRA), has been developed. The i-MRA employs two techniques to reduce the number of different structural types within the gridshell.

The first technique, known as Multiple Order MRA (MO-MRA), involves an iterative process to minimize *loose elements*. Initially, the hanging network configuration is computed using the classical MRA with ropes of length $l_{rope,1}$. If *loose ropes* are present in the final configuration, the MO-MRA assigns a new target length $l_{rope,2} < l_{rope,1}$ to these *loose ropes*. The hanging network equilibrium configuration is

then recomputed. This process is repeated: if *loose ropes* still exist, a new target length $l_{rope,3} < l_{rope,2}$ is assigned, and the equilibrium configuration is recomputed. The iteration continues until the structural form is nearly free of *loose elements*.

From a computational point of view, this method involves modifying Eq. (2) to account for different forces F_{rope} exerted by the ropes, depending on the category of elements to which they belong. Given that there are w categories, Eq. (2) can be rewritten as follows:

From a computational point of view, this method involves modifying Eq. (2) to account for different forces F_{rope} exerted by the ropes, depending on the category of elements to which they belong. Here, element categories refer to groups of structural elements with the same target length $l_{rope,i}$. Given that there are w such length-based categories, Eq. (2) can be rewritten as follows:

$$\begin{cases} F_{rope} = k(l - l_{rope,1}) & \text{if } \; l \geq l_{rope,1} \\ F_{rope} = 0 & \text{if } \; \gamma(l_{rope,1} - l_{rope,2}) + l_{rope,2} < l < l_{rope,1} \\ F_{rope} = k(l - l_{rope,2}) & \text{if } \; l_{rope,2} < l \leq \gamma(l_{rope,1} - l_{rope,2}) + l_{rope,2} \\ \quad \dots & \quad \dots \\ F_{rope} = k(l - l_{rope,w}) & \text{if } \; l_{rope,w} < l \leq \gamma(l_{rope,(w-1)} - l_{rope,w}) + l_{rope,w} \\ F_{rope} = 0 & \text{if } \; l < l_{rope,w} \end{cases} \tag{10}$$

In Eq. (10), the coefficient $\gamma \in (0, 1)$ is a user-defined parameter that allows for prioritizing loose ropes belonging to one category over another.

The second method that defines i-MRA is called Repulsive Nodes MRA (RN-MRA). This method is applied after MO-MRA, particularly when loose elements constitute a small portion of the total structural elements. RN-MRA introduces a repulsive force field between the nodes, causing them to move apart and tension the slack ropes.

Mathematically, this involves adding a new term, $\vec{q}$, representing the repulsive force field, to Eq. (1), resulting in the following updated equilibrium equation:

$$\vec{R}_i = \vec{p}_i + \vec{q}_i + \sum_{j=1}^{n_i} \left\{ \vec{F}_{rope,ji} \right\} - c_i \cdot \vec{v}_i - m_i \cdot \vec{a}_i = 0 \tag{11}$$

The repulsive force field is defined as proportional to the distance l_{ij} between two adjacent nodes i and j. Specifically, by defining k_{rep} as the proportionality coefficient for the repulsive forces, the force acting on the two nodes can be expressed as:

$$\vec{q} = -k_{rep}(\vec{l_{rope}} - \vec{l_{ij}}) \tag{12}$$

The application of the repulsive force field has the effect of significantly reducing the number of *loose ropes*, thereby minimizing the variety of structural elements needed to define the shape of the gridshell. However, it is important to note that the repulsive forces do not represent an actual load condition that the structure will face during its service life. As a result, applying the repulsive force field introduces a deviation from the funicular configuration of the structure. While this method enhances the constructibility of the structure, it compromises its structural behaviour. Therefore, RN-MRA should be applied with caution, ideally when the equilibrium condition features only a small number of *loose elements*.

In conclusion, the combination of MO-MRA and RN-MRA enables the definition of a structural form characterized by a reduced number of structural element types. This optimization streamlines the construction process and enhances practical feasibility. The workflow for implementing the i-MRA methodology is depicted in Fig. 2.

In the workflow, starting from the geometric configuration of the gridshell defined using the pure MRA method, a set of target lengths is assigned to the cables that form the hanging net model, which represents the inverse geometric configuration of the structure. At this stage, a second target length is assigned based on the distance l, as defined in Eq. (10), and the new equilibrium configuration is computed. The process is then iterated, recalculating the equilibrium configuration for each newly assigned target length. Finally, a repulsive force field is applied to introduce minor adjustments to the gridshell, subtly altering its shape relative to the funicular configuration while further reducing the variety of structural elements.

3. Multi-objective optimization problem definition

In Section 2.2, the i-MRA form-finding method was presented, enabling the definition of a structural form that optimizes both structural efficiency and constructability.

The proposed optimization framework relies on two distinct sets of user-defined variables: hyperparameters and design parameters. Hyperparameters refer to the user-defined settings that govern the behaviour of both the form-finding and optimization algorithms. In the presented framework, this category comprises the dynamic variables of the hanging network system, including nodal masses, damping coefficients, and external nodal loads. Although these hyperparameters are defined a priori and are not directly optimized, their correct definition is essential for ensuring numerical stability and convergence. A proper balance between these variables is fundamental to accurately computing the equilibrium configuration of the hanging net. For example, the elastic coefficient and damping coefficient critically influence the convergence behaviour of the model, while the forming load p directly affects the final gridshell geometry. Design parameters, in contrast, are the variables actively optimized in the framework. These are represented by the vector of target lengths $L_{rope} = [L_{rope,1}, L_{rope,2}, \dots, L_{rope,N}]$, which define the lengths of the structural elements. Adjusting these parameters allows for the generation of various structural geometries with differing degrees of constructability and structural efficiency. Traditionally, these design parameters would be selected manually through trial-and-error. In this work, however, an automatic selection approach through the solution of a multi-objective optimization problem is proposed, significantly improving the efficiency and effectiveness of the design process.

Multi-objective optimization problems aim to find an optimal solutions by simultaneously considering conflicting objective functions [53]. The goal of this approach is to achieve a balance between the multiple performance criteria of the system, such as structural efficiency, constructability, and cost. The problem can be generally formulated as follows:

$$\begin{aligned} &Find \; \vec{x} = [x_1, \dots, x_n]^T \in \Omega \subseteq \mathbb{R}^n \; such \; that \\ &\min_{\vec{x}} \vec{f}(\vec{x}), \quad \text{where } \vec{f}(\vec{x}) = [f_1(\vec{x}), \dots, f_m(\vec{x})]^T \in \mathbb{R}^m \\ &\text{s.t.} \quad g_q(\vec{x}) \leq 0 \qquad \forall q = 1, \dots, n_q, \\ &\qquad h_r(\vec{x}) = 0 \qquad \forall r = 1, \dots, n_r, \end{aligned} \tag{13}$$

In this problem formulation, the vector of design variables $\vec{x}$ has dimensions n, each constrained by box constraints $x_i^l \leq x_i \leq x_i^u$, commonly referred to as side constraints. Additionally, the objective functions vector $\vec{f}(\vec{x}) = [f_1(\vec{x}), \dots, f_m(\vec{x})]^T$ is composed of m components.

The problem includes inequality constraints $g_q(\vec{x}) \leq 0$, which must be satisfied for all $q = 1, \dots, n_q$, where n_q represents the total number of inequality constraints. Similarly, the equality constraints $h_r(\vec{x}) = 0$ ensure that specific conditions are met for all $r = 1, \dots, n_r$ with n_r representing the total number of equality constraints. In practical applications objective functions are often conflicting, making it impossible to minimize all objectives simultaneously. This inherent conflict means that an optimal solution for multi-objective optimization problems is not always straightforward. When considering multiple objectives, no single solution may completely outperform others; instead, optimality is attained through a balance among the competing objectives.

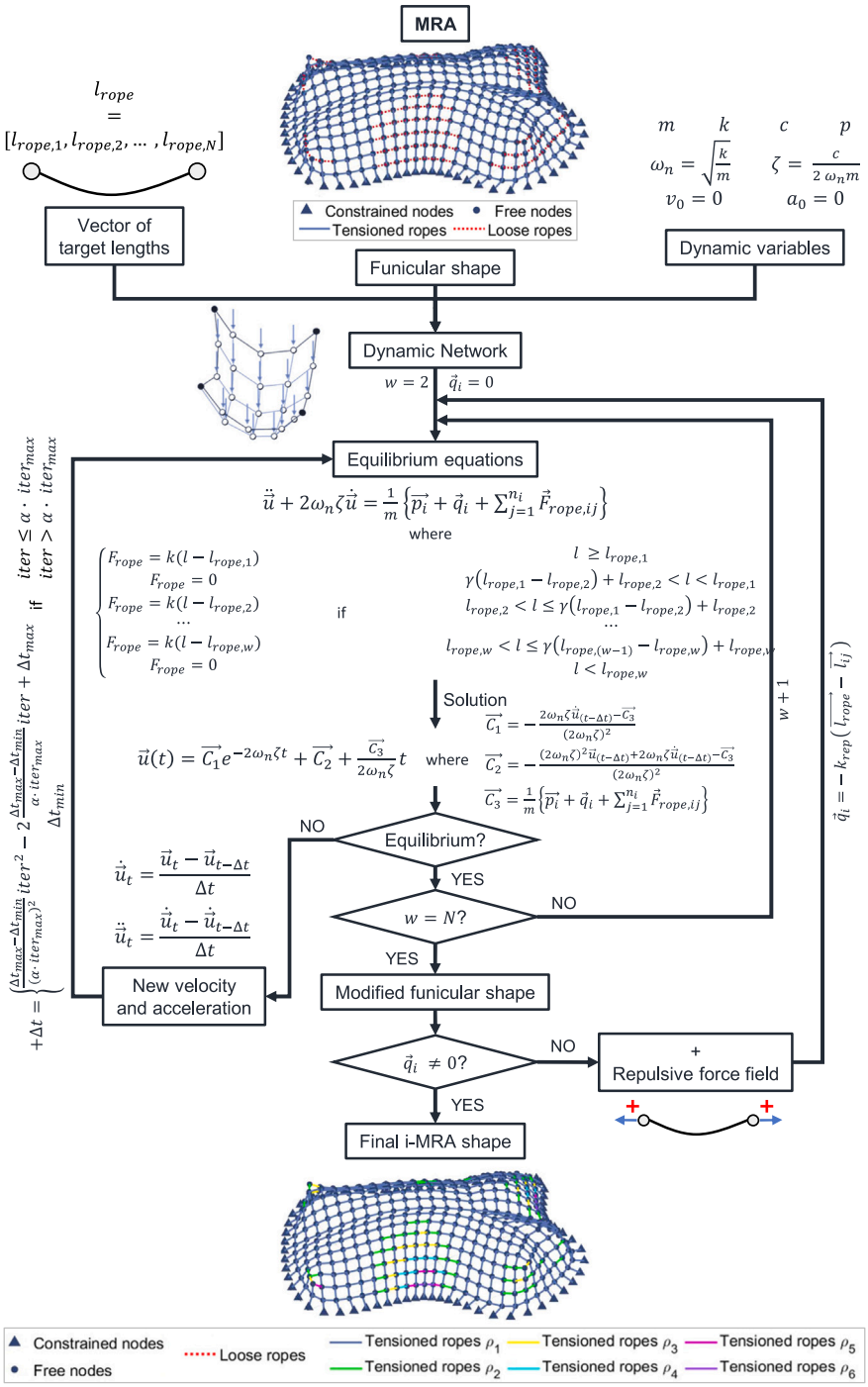

Fig. 2. i-MRA workflow.

Evaluating the quality of solutions in multi-objective optimization requires careful assessment of the objective functions. Due to the partial ordering of the feasible set, it is not possible to directly compare two solutions unequivocally. Each solution might excel in different objective aspects, necessitating a trade-off to identify the most balanced and acceptable solution. This trade-off reflects the complexity and the need for a nuanced approach in determining optimality in multi-objective contexts.

To evaluate the quality of solutions in a minimization problem, the *Pareto dominance* is utilized.

A solution $\vec{u} = F(\vec{x})$ *Pareto dominates* $\vec{v} = F(\vec{x}')$ (denoted $\vec{u} \prec \vec{v}$) if:

$$\begin{aligned} &u_i \leq v_i \quad \forall i = 1, \dots, m, \\ &\exists j \in \{1, \dots, m\} : u_j < v_j. \end{aligned} \tag{14}$$

In words, $\vec{u}$ dominates $\vec{v}$ if it is equal or better in all objectives and strictly better in at least one.

A solution $\tilde{\vec{x}}$ is *Pareto optimal* if no other feasible solution $\vec{x} \in \Omega$ exists such that $F(\vec{x})$ Pareto dominates $F(\tilde{\vec{x}})$. The set of all Pareto optimal solutions forms the *Pareto optimal set*:

$$\mathbf{P} = \left\{ \tilde{\vec{x}} \in \Omega \,\middle|\, \nexists\, \vec{x} \in \Omega \text{ with } F(\vec{x}) \prec F(\tilde{\vec{x}}) \right\}. \tag{15}$$

The corresponding objective space representation is the *Pareto front*:

$$\mathbf{P_F} = \left\{ \vec{u} = F(\vec{x}) \,\middle|\, \vec{x} \in \mathbf{P} \right\}. \tag{16}$$

3.1. Design variables

In the context of the multiobjective optimization problem, the design variables $\vec{x} = [x_1, \ldots, x_n]^T \in \Omega$ are the parameters or features of a system or model that can be controlled, adjusted, or modified within specified limits to achieve the desired objectives. Design variables are the foundational elements that define the search space Ω of an optimization problem. Their values determine the configuration and performance of the system being optimized.

Selecting parameters for the i-MRA form-finding method, as discussed in Section 3, can be a challenging task. Typically, this selection is based on the expertise of the user, who must try multiple combinations of target lengths to find the optimal set. The parameters that most influence the outcome of the i-MRA, specifically the structural forms, are the target lengths of the slack ropes $L_{rope} = [L_{rope,1}, L_{rope,2}, \ldots, L_{rope,N}]$. By varying these target lengths, it is possible to obtain structural shapes with different degrees of slackness, structural behaviour, and constructability.

This work aims to leverage on an optimization algorithm to automate the selection of the target lengths. This automation enables the calculation of the parameters necessary to achieve the optimal structure. Consequently, the structural form is optimized through an automated process, eliminating the need for the user to have the expertise to select the optimal combination of the parameters.

3.2. Constraints

In general, the objective of structural optimization problems is to identify the optimal structural configuration that is able to withstand the design loads. In this context, it is essential that the different solutions assessed during the optimization process are evaluated by performing structural verifications.

To achieve this, a finite element model is developed based on the derived structural shape, utilizing Circular Hollow Section (CHS) profiles constructed from S355 steel. Finite element analyses are performed using a custom MATLAB code [54,55] to calculate nodal displacements and stress characteristics for each beam. These results are then used to verify whether the generated structure meets the required structural verifications.

This work aims to define a method to assist the designer in defining a preliminary structural form during the conceptual design phase. At this stage, simplified structural verifications are performed. Specifically, the method ensures that the gridshell structure meets the maximum vertical displacement, material yield strength, and Euler buckling criteria for linear structural elements, as indicated by Eq. (17).

$$\delta_{max} < \delta_{lim} \qquad |\sigma_{max}| < f_y \qquad N_{max}^{Compression} < N_{Buckling} \tag{17}$$

where δ_{max} represents the highest nodal displacement in the structure, and δ_{lim} is set to $\frac{1}{250}$ of the structure largest dimension without external constraints. The term $|\sigma_{max}|$ denotes the absolute maximum stress in the structure, which must be less than f_y, the yield stress of the steel used. Lastly, $N_{max}^{Compression}$ is the maximum compressive axial force, and $N_{Buckling}$ is the critical axial force for Euler buckling.

In the context of classical notation used in structural optimization problems, inequality constraints are typically expressed as $g_q(\vec{x}) \leq 0$. Accordingly, the equations in Eq. (17) can be reformulated as:

$$\frac{\delta_{max}}{\delta_{lim}} - 1 < 0 \qquad \frac{|\sigma_{max}|}{f_y} - 1 < 0 \qquad \frac{N_{max}^{Compression}}{N_{Buckling}} - 1 < 0 \tag{18}$$

The constraints presented above represent a simplified approach to structural verification, suitable for the conceptual design phase. However, it is well established that buckling is a critical constraint in the design and optimization of gridshell structures. Accurately estimating the buckling capacity of such systems is a complex task, as demonstrated in several studies [56–58]. The buckling behaviour of gridshells is governed by both local and global instability mechanisms, which often interact in a nonlinear manner. Capturing these effects requires advanced numerical analyses that account for geometric nonlinearity (GNIA) and, in many cases, material nonlinearity (GNMIA). The necessity of such approaches has been extensively discussed in the Draft Guide to Buckling Load Evaluation of Metal Reticulated Roof Structures by Working Group 8 of the International Association for Shell and Spatial Structures [59], where it is explicitly stated that linear buckling analyses alone are inadequate for gridshell assessment. The guide suggests that for double-layer gridshells, a linear buckling analysis may provide a preliminary estimate of structural stability. However, due to the significant uncertainties associated with this approach, very high safety factors are required. Such high safety factors are incompatible with the principles of structural optimization, as they would lead to a substantial underestimation of the critical load, resulting in overly conservative and potentially suboptimal design solutions. More critically, the guidelines indicate that for single-layer gridshells, the discrepancies between linear buckling predictions and real structural behaviour are so pronounced that simplified approaches cannot be adopted. In these cases, a nonlinear approach that consider geometric and material nonlinearity, along with the effects of construction imperfections, becomes mandatory. A rigorous buckling analysis should also consider not only global instabilities but also the influence of local imperfections. Previous research has shown that material nonlinearities and geometric imperfections can significantly reduce the actual buckling capacity of gridshells [58]. For this reason, advanced studies often employ Monte Carlo simulations to define defect patterns and evaluate structural behaviour under a wide range of imperfection scenarios [60]. The integration of such analyses within an automated optimization framework would lead to a substantial increase in computational cost, making the approach impractical for early-stage design exploration. Given these complexities, the present study adopts a simplified buckling evaluation, focusing on local buckling of individual members rather than a full-scale global buckling analysis. While this approach does not capture all the instability phenomena that may arise in gridshell structures, it is deemed appropriate for the conceptual design phase, where the objective is to generate preliminary structural forms rather than to perform final design verifications. A comprehensive buckling analysis, including GNIA and GNMIA, should be carried out in later design stages to fully account for all structural constraints, material properties, and imperfection effects.

3.3. Objective functions

In this work, two optimization objective functions have been defined. The first objective function, f_1, corresponds to the number of distinct structural elements that constitute the gridshell. The goal is to minimize f_1 as much as possible, as it is directly related to the simplicity of the structure assembly. A smaller number of structural elements with different lengths facilitates the management of both the manufacturing and assembly phases, thereby streamlining the entire construction process.

In contrast, the second objective function, f_2, is related to the consumption of material for the structure. The minimization of construction material is obviously closely linked to the final cost of the gridshell. In fact, the less material used, the lower the overall economic and environmental cost of the structure. In general, calculating the net amount of material required for the structure is relatively straightforward. This involves multiplying the length of each element by its cross-sectional area A and summing these values. However, this approach does not account for material waste generated during

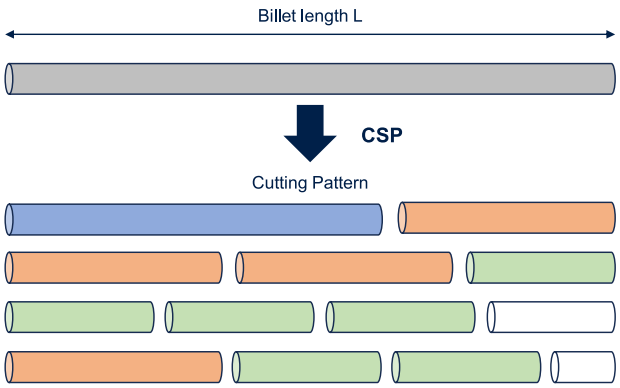

Fig. 3. Representation of the Cutting Stock Problem (CSP).

the production of the structural elements. The gross material consumption, which includes this waste, can significantly differ from the net consumption. Accounting for this discrepancy is crucial, as it can substantially affect the results of the optimization problem.

The structural steel elements used in gridshell-type structures are produced from billets of constant length, typically 12 m, for transportation reasons [61]. These billets are then cut into various lengths to produce the desired structural elements generating industrial waste. Managing this material scrap is a well-documented industrial problem referred to in the literature as the Cutting Stock Problem (CSP).

3.3.1. Production wastes minimization through Cutting Stock Problem (CSP)

The Cutting Stock Problem (CSP) [62] is a prevalent issue in logistics and industrial applications. In operations research, CSP involves cutting standard-sized pieces of stock material, such as metal billets, into specified lengths while minimizing material waste. This optimization problem is widely encountered across various industrial sectors.

The core concept of CSP is that billets of equal lengths are available and need to be cut into pieces of different lengths. In Fig. 3 is reported a representation of the Cutting Stock Problem (CSP), illustrating a billet with various cutting patterns. The image depicts how raw material is divided into smaller pieces to optimize usage and minimize waste, showcasing different possible cutting configurations. The objective of CSP is to determine the most efficient cutting patterns to minimize waste.

In the context of a one-dimensional CSP, with a homogeneous set of billets (of equal size), it is possible to define the following problem parameters:

- A set of m billets B, where each billet has a length L.
- A set I of required piece with lengths l_i and their corresponding quantities d_i, for $i = 1, \dots, n$.

Here, m represents the number of available billets, while n denotes the number of pieces that need to be produced.

The problem is also characterized by two different decision variables:

- $x_{i,b} \in 0, 1$: unitary if the item i is allocated to the billet b, equal to 0 otherwise.
- $y_b \in 0, 1$: unitary if the bille b is utilized, equal to 0 otherwise.

The objective is to minimize the number of billets used:

$$\min \sum_{b \in B} y_b \tag{19}$$

Under the constraints:

1. Avoid multiple allocation of the items:

$$\min \sum_{b \in B} x_{i,b} = 1 \quad \forall i \in I \tag{20}$$

2. Billet length constraints:

$$\min \sum_{i \in I} L_i x_{i,b} \leq L y_b \quad \forall b \in B \tag{21}$$

3. The item can be assigned to a billet if and only if the billet is already in use:

$$x_{i,b} \leq y_b \quad \forall i \in I, \forall b \in B \tag{22}$$

The problem has been defined in such a way that each piece must be assigned to a billet. Furthermore, the sum of the lengths of the pieces assigned to a billet must not exceed the length of the billet itself. Finally, a piece may be assigned to a billet if and only if that billet is in use.

The Cutting Stock Problem (CSP) can be formulated as an integer linear programming (ILP) problem. A practical procedure to solve this problem was proposed by [48,63]. Instead of generating every possible cutting pattern, it is more efficient to generate patterns dynamically by solving a subproblem.

The process begins with a base set of cutting patterns. The ILP is then solved to minimize the number of billets used while ensuring that the current cutting patterns satisfy the demands. After solving this initial problem, a new cutting pattern is generated by addressing an integer linear programming subproblem.

This subproblem involves finding the optimal new pattern, defined by the number of cuts from each length that total no more than the billet length. The objective is to minimize the reduced cost of the new pattern, calculated as one minus the sum of the Lagrange multipliers for the current solution multiplied by the new cutting pattern. If this reduced cost is negative, incorporating this pattern into the ILP will improve the objective. If no negative reduced cost pattern exists, the current patterns yield the optimal solution. This stopping criterion parallels the termination condition of the primal simplex method, which stops when no variable has a negative reduced cost.

In this work, the cutting stock problem (CSP) was integrated into an optimization framework with two objectives. The first objective was to minimize the waste generated during the industrial production of structural elements. The second objective aimed to account for this waste to accurately calculate the gross amount of material required for the construction of the structure. A MATLAB code, available at MATLAB CSP Solver, was utilized for this purpose. This code employs the linear programming method previously described to solve the CSP effectively.

3.4. The search engine: Multiobjective genetic algorithm (NSGA II)

In this work, the MATLAB function *gamultiobj* [64] is employed to address the multi-objective optimization problem. This function is based on the Non-dominated Sorting Genetic Algorithm II (NSGA-II) [42,65], a specific type of multi-objective genetic algorithm (MOGA).

The NSGA-II algorithm operates on a population of potential solutions, evolving them over several generations to approximate the Pareto set. Initially, a diverse population is generated randomly. This enhances the exploration in the early stages of optimization. Each solution is evaluated based on its performance across multiple objectives, with non-dominated sorting used to rank them into Pareto fronts [66]. The best non-dominated solutions form the first front.

Tournament selection is applied during the selection process [67,68]. This method chooses individuals for reproduction based on their Pareto rank and crowding distance. It maintains diversity by favouring solutions in less crowded regions of the objective space. Genetic operators like simulated binary crossover and polynomial mutation introduce variability, enabling thorough exploration of the search space.

Elitism [69] is crucial in the algorithmic process. It preserves the best solutions from each generation, maintaining high quality over successive iterations. Using *gamultiobj* helps obtain a diverse set of solutions that represent the trade-offs among different objectives. This approach enables informed decision-making based on a comprehensive understanding of possible optimal solutions.

3.5. Optimization workflow: the unconstrained optimization problem

Fig. 4 shows the workflow adopted for the form discovery and optimization process.

The workflow begins with the initial definition of a starting grid or mesh. At this stage, the Multi-Objective Genetic Algorithm (MOGA) generates a population where each individual is represented by a distinct vector of lengths, denoted by $L_{rope,i} = [L_{rope,1,i}, L_{rope,2,i}, \dots, L_{rope,N,i}]$. These vectors represent the parameters of the i-MRA form-finding method.

For each individual in the population, form-finding with i-MRA is performed to determine the structural form of the gridshell, as depicted in the left part of Fig. 4. The resulting form is structurally efficient concerning the loads applied during the form-finding process. All the obtained shapes are then used to define finite element models. In this case, the models are defined in structural steel and are subjected to a self-weight load added to concentrated loads on the structural nodes. For the size of the structural elements, the Circular Hollow Section (CHS) profile list is adopted, which include the values of the cross-sectional area A and bending inertia J for each profile. In the first step, it is assumed that the structural elements cross-section is the smallest profiles in the list.

The next step involves conducting a structural analysis for each configuration to ensure compliance with the given constraints. In the workflow shown in Fig. 4, this process is represented as a loop in which finite element analysis (FEA) is performed to calculate internal forces, followed by structural verification checks.

For configurations that do not satisfy the constraints, the profile dimensions are iteratively increased until an appropriate Circular Hollow Section (CHS) profile is identified that meets the structural requirements. This iterative approach determines the minimum required cross-sectional area A for the structural elements, ensuring both efficiency and compliance with design criteria.

Once all generated solutions have been verified, the objective functions can be evaluated. After the form-finding process, the length of each structural element is determined, allowing for the calculation of Objective Function 1, as outlined in the workflow in Fig. 4.

Next, the Cutting Stock Problem (CSP) is solved to estimate the number of billets required to produce these elements. By multiplying the number of billets by their length and by the cross-section area defined in the structural analysis, the total material required for the structure, denoted as W_{gross}, is computed. This value is identified as Objective Function 2 in the workflow in Fig. 4.

Finally, the fitness function evaluated by MOGA considers two key components: (1) the number of distinct structural element types (n_{type}) based on varying lengths, and (2) the total material consumption (W_{gross}). These factors collectively guide the optimization process towards efficient and sustainable structural solutions.

At this stage, the individuals are ranked using a non-dominated sorting mechanism to identify the Pareto fronts within the space of the objective functions. Based on their rankings, MOGA combines the individuals to generate a new population and iterates the process. This process continues until the final Pareto front, consisting of non-dominated solutions, is defined, as reported on the right in Fig. 4. These solutions are optimized with respect to the two analysed objective functions.

The proposed method transforms a constrained multiobjective optimization problem into an unconstrained one, albeit with some costs. This transformation requires introducing a prior assumption: that increasing the cross-sectional dimension of the structural elements will always yield a structural solution that meets the constraints. Nonetheless, in the context of this study, this assumption is not overly restrictive and can be considered generally valid.

The decision to transform the problem into an unconstrained optimization problem is driven by computational cost considerations. The form-finding method involves iteratively solving a highly nonlinear system, which is computationally intensive. In contrast, as this study focuses on the preliminary design of gridshells, structural analyses are performed within the linear elastic field. Consequently, the form-finding process is several orders of magnitude more computationally demanding than FEM analyses.

By transforming the method from constrained to unconstrained, one design variable, the cross-sectional dimension of the structural elements, is eliminated. This reduction in the domain search space allows for fewer individuals to be analysed while maintaining the same level of exploration. However, this benefit comes at the cost of an increased number of FEM analyses. Since, each individual requires repeated analysis until a cross-section that satisfies the structural constraints is identified.

As previously mentioned, the computational cost of FEM analyses is several orders of magnitude lower than that of form-finding. Therefore, it is cost-effective to reduce the number of individuals whose form is defined by form-finding, even if this significantly increases the number of FE analyses.

It is important to note that the overall optimization workflow involves several computationally demanding steps. The approach integrates a nonlinear form-finding process using the i-MRA, which solves the dynamic behaviour of the multi-body hanging network, an elastic-linear FEM analysis to verify structural constraints, and the solution of the Cutting Stock Problem (CSP) via linear programming for gross mass optimization. While these components can be computationally intensive, several strategies have been implemented to ensure practical computation times even on standard hardware. The FEM analysis has been simplified by using streamlined structural verifications, reducing verification times to a few seconds per iteration. Additionally, parallel computing has been employed to evaluate multiple solutions concurrently, and the cross-sectional properties of the structural elements have been standardized to use a single billet type for CSP optimization. These measures collectively reduce the computation time for each CSP solution to only a few seconds. By addressing computational efficiency, the proposed method enables rapid parametric studies and ensures that the workflow remains feasible for conceptual design applications. In real-case applications, where only a single optimization run may be required, further refinements, such as more detailed structural verifications or the use of variable cross-sections, would increase computational costs. However, the computation time would remain within a range that allows the method to be practically applicable.

4. Optimization results and discussion

Three different case studies are presented in this section. The case studies are of increasing complexity in order to evaluate the performance of the proposed method on different structural forms.

In all case studies, the form-finding process is obtained using gravitational loads by masses concentrated at the grid nodes. While the method also supports the application of external nodal forces, these were not employed in this study, as the primary objective was to define structural geometries optimized specifically for vertical loads. This approach simplifies real-world loading conditions, where forces may be applied as nodal loads or distributed along beam elements, but it ensures a robust and computationally efficient form-finding process.

During the structural analysis phase, a more refined loading scheme is implemented: the self-weight is modelled as a uniformly distributed load along the beam elements, while the nodal overloads are applied as constant forces at each node. The structural verification under these loading conditions serve as constraints in the optimization process, ensuring that the final design meets predefined structural requirements.

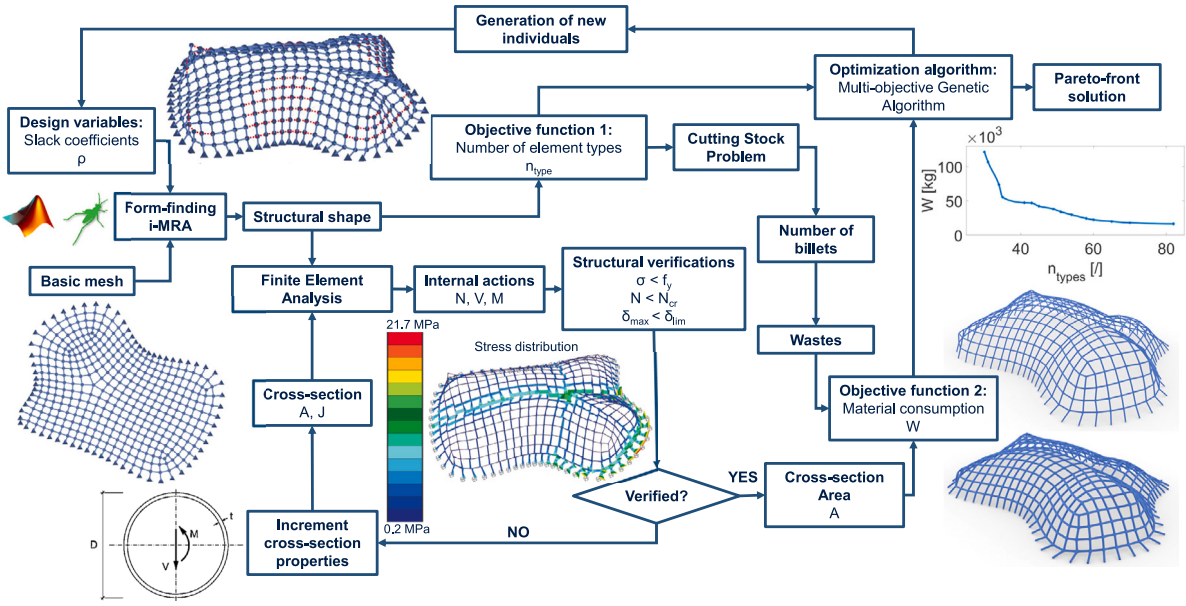

Fig. 4. Optimization procedure workflow.

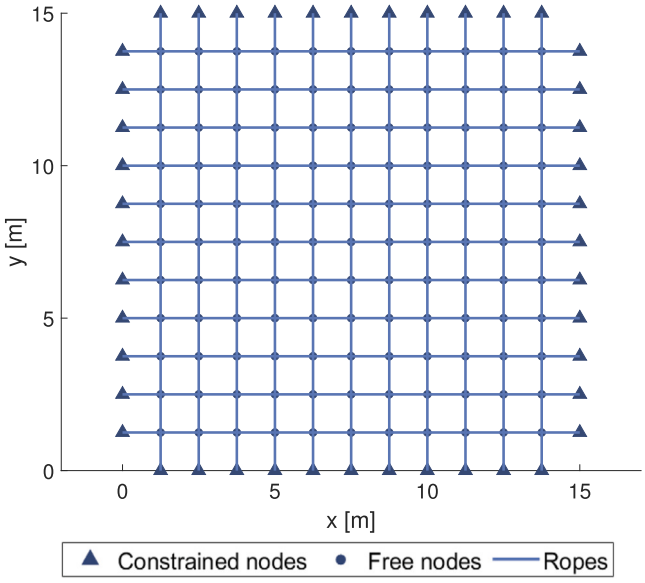

Fig. 5. Base mesh for the simple and regular quadrangular gridshell structure.

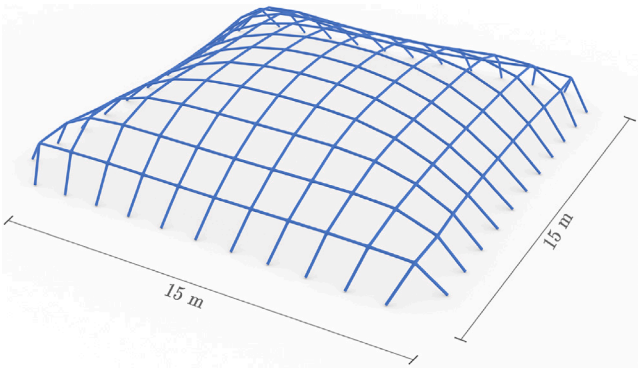

Fig. 6. Square mesh gridshell with a side length of 15 m.

4.1. Multiobjective optimization of simple square mesh gridshell

The first case study involves a square base gridshell with a side length of 15 m, as shown in Fig. 5. The application of the i-MRA to this very simple case study results in the shaper represented in Fig. 6. This basic case study serves as a reference point to evaluate the results of the method.

The optimization is performed by considering the gridshell under its own weight and various nodal overloads to assess the effect of the loads on the structural shape. Specifically, nodal overloads of 1 kN, 5 kN, 10 kN, and 50 kN were considered. These values are notably higher than those typically used in standard design practice. However, in this study, a parametric analysis on academic case studies is performed. Therefore, high overloads are intentionally employed to induce significantly different structural shapes and dimensions. The primary aim is to demonstrate the optimization methodology, using these case studies as tests rather than practical applications.

Fig. 7 displays the optimization results for nodal overloads equal to 1 kN, 5 kN, and 10 kN.

In Fig. 7, the quantities W_{gross} and W_{net} represent, respectively, the total and net weight of steel (in kilogrammes) required for constructing the structures, while the variable n_{type} denotes the number of distinct structural element types, corresponding to the different lengths needed for their production.

The results are presented as histograms, considering one or two design variables. The graphs represent how optimization outcomes vary when the objective is to minimize either net or gross material. The gross material consumption W_{gross} was obtained by the application of the CSP. Calculating material consumption using the CSP results in a reduced variety of optimal solutions. This occurs because solutions with different net material consumptions W_{net} may, in practice, require the same total material when production waste is considered. This highlights the critical importance of accounting for production waste in determining truly optimal solutions in real-world applications, where waste is a not negligible component.

Fig. 7(a) and (c) show material minimization, accounting for production waste. In contrast, Fig. 7(b) and (d) focus on net material consumption.

The optimization results for the case study with a nodal overload of 50 kN are shown in Fig. 8. The solutions are presented in the objective function space as Pareto fronts. The comparison of optimization

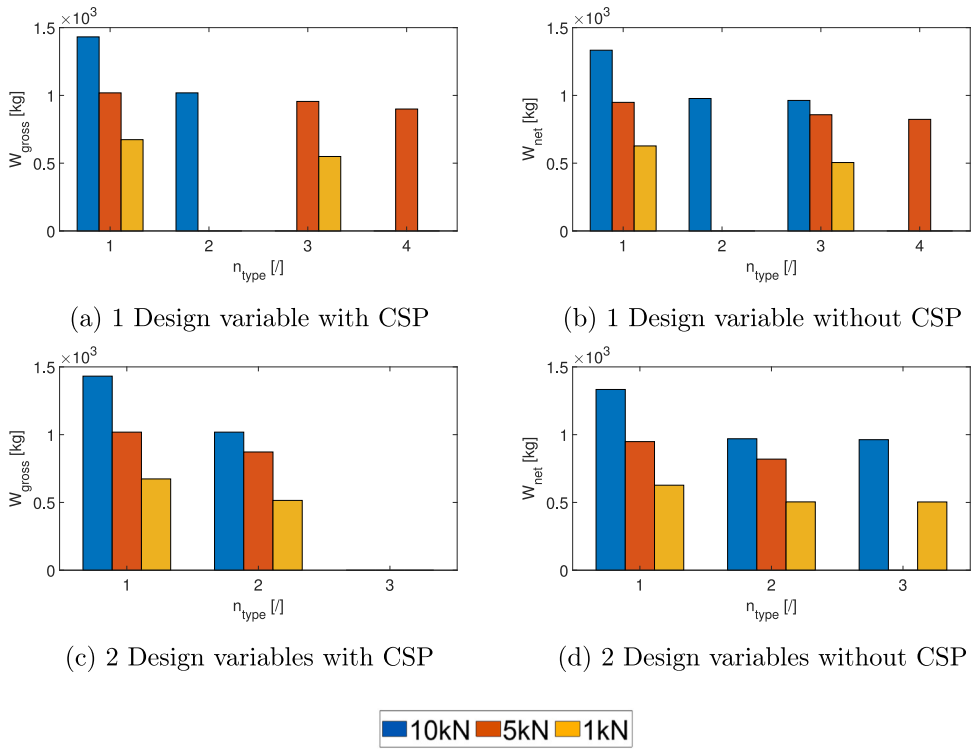

(a) 1 Design variable with CSP (b) 1 Design variable without CSP

(c) 2 Design variables with CSP (d) 2 Design variables without CSP

Fig. 7. Quadrilateral gridshell optimization results considering one or two design variable and comparing the differences in minimizing net or gross material consumption.

Table 1
Quadrilateral gridshell optimization results in terms of use of material [kg] and construction complexity expressed as n_{type}.

	n_{type}	CSP: W_{gross}				No CSP: W_{net}			
		50 kN	10 kN	5 kN	1 kN	50 kN	10 kN	5 kN	1 kN
1 var	1	7131	1432	1019	673	6641	1333	949	627
	2	3905	1019	\	\	3773	977	\	\
	3	\	\	956	549	\	963	857	505
	4	3330	\	900	\	\	\	823	0
	5	2683	\	\	\	2698	\	\	\
	7	\	\	\	\	2659	\	\	\
	9	\	\	\	\	2589	\	\	\
2 var	1	7131	1432	1019	673	6641	1333	949	627
	2	2552	1019	872	515	2492	970	820	504
	3	\	\	\	\	\	963	\	504

results includes both scenarios: accounting for production waste and considering only the net consumption of structural material. The Fig. 8 visually represents the optimal solutions within the Pareto set. It shows that flatter structural configurations require thicker elements to withstand higher compressive forces but can be built with fewer types of structural members. In contrast, less flat configurations use a wider variety of structural members, allowing for the use of more slender elements.

It can be observed that the number of different types of structural elements is inversely proportional to the amount of material required to assemble the gridshell. This indicates that the chosen objective solutions are conflicting. Consequently, there is no single globally optimal solution. Instead, there is a set of optimal solutions from which the designer can select the most suitable compromise to meet the specific project requirements. This set of solutions consists of the non-dominated solutions found on the Pareto front.

In this scenario, the gridshell exhibit notable differences in both shape and the thickness of their structural elements. The structures with a lower number of element typologies display a low-profile configuration characterized by substantial compressive forces, necessitating thick structural elements of uniform length. In contrast, the lighter structures depicts a significantly taller configuration achieved through the use of two distinct types of thinner structural elements.

Therefore, the designer has the option to choose between two markedly different types of structures and can select the best compromise that suits the specific project requirements.

It is worth emphasizing that incorporating gross mass optimization (W_{gross}) from the very early stages of conceptual design offers significant advantages over relying solely on net mass optimization (W_{net}). Although optimizing for W_{net} can yield designs that are theoretically material-efficient, such configurations may ultimately prove impractical when production waste is taken into account. In fact, as demonstrated in Fig. 8, while many geometries are common to both optimization objectives, certain configurations that appear optimal when considering only the net mass do not translate into distinct solutions under gross mass optimization. For instance, configurations characterized by $n_{type} = 7$ and $n_{type} = 9$ are absent in the gross mass results because, in practice, their total material consumption (including waste) is equivalent to that of other designs. By evaluating gross mass early on, the proposed approach directs the project towards geometries that are not only structurally efficient but also aligned with industrial production processes, thereby reducing the likelihood of costly redesigns in later stages.

Finally, the results for this simple case study are summarized in Table 1. The table displays the material consumption in kilogrammes for solutions with varying degrees of construction complexity. Complexity is indicated by the number of different types of elements required to build the structure n_{type}. The results are given for different nodal overloads.

It can be observed that the number of different types of structural elements is inversely proportional to the amount of material required to construct the gridshell. This indicates that the chosen objective solutions are conflicting.

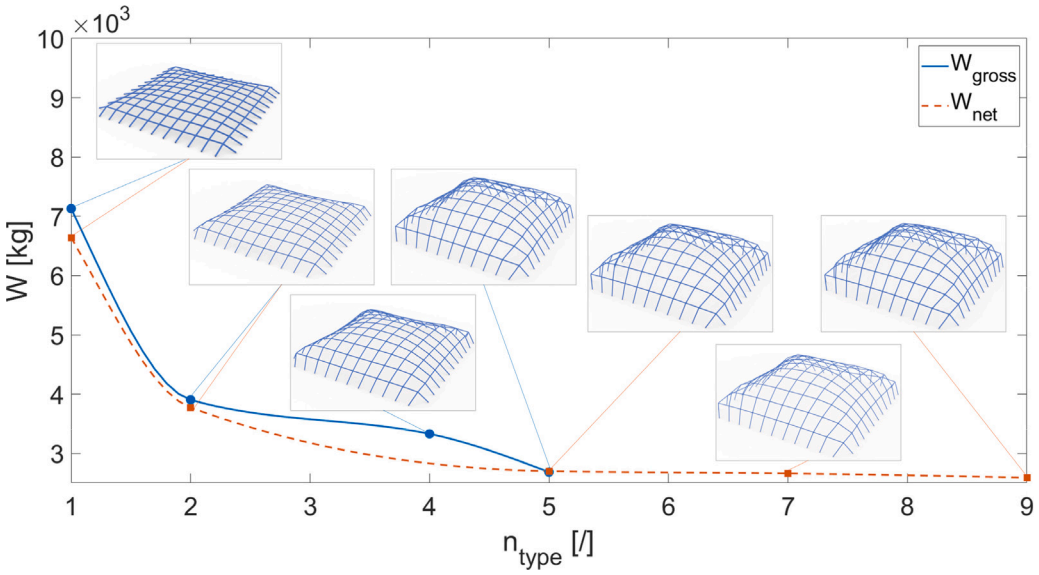

Fig. 8. Quadrilateral gridshell optimization results considering a nodal overload of 50 kN and 1 design variable. Results represented as Pareto fronts in the objective functions search space.

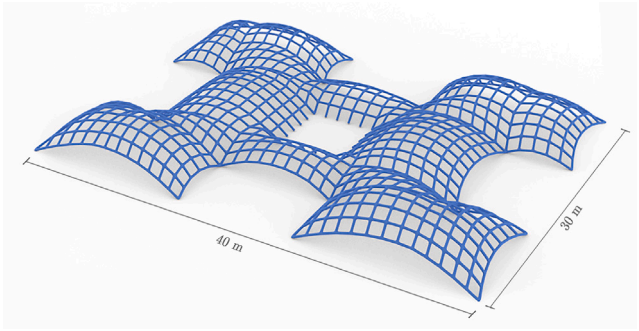

Fig. 9. Complex but regular gridshell structure.

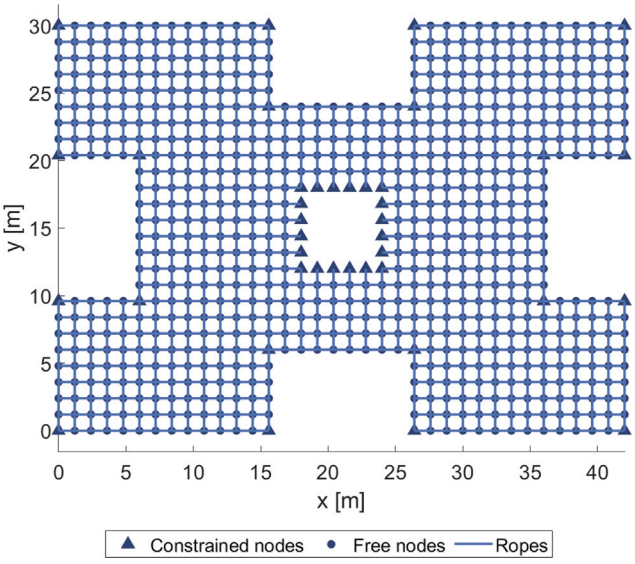

Fig. 10. Base mesh for the complex but regular gridshell structure.

4.2. Multiobjective optimization of complex but regular gridshell structure

In the second case study, the complexity is increased by investigating the behaviour of a more complex shape, as depicted in Fig. 9. This structure is composed by five distinct zones. The central part features a large rectangular room with a square opening in the middle. Surrounding the central zone are four smaller rectangular areas, each connected to the corners of the main zone. This configuration introduces additional geometric and structural challenges, providing a more robust test of the optimization method.

The basic mesh used to define this structure comprises 760 nodes connected by 1420 linear elements, each with a length of 1.20 m. The structure is constrained at the corners of the outer perimeter and along the edges of the central square opening (see Fig. 10).

The structure was optimized by considering up to two design variables, which represent the L_{rope} target lengths used during the shape-finding process. Furthermore, the case in which the optimization is performed using two design variables and employs the Repulsive Nodes Multibody Rope Approach is analysed. The analyses are performed considering the same load cases as in the first case study, namely the structure self-weight and various magnitudes of nodal loads. As with the first case, the results are reported in terms of both minimizing the net consumption of structural material and the gross consumption calculated by the use of the CSP. The results of the optimization are reported in Table 2.

The results are also presented as histograms in Fig. 11, illustrating the relationship between material consumption and the types of structural elements. This provides the designer with various design solutions, depending on whether the objective is to minimize material consumption or construction difficulty. The graphs demonstrate the impact of varying the number of design variables and the use or non-use of the Repulsive Nodes method. The left-side graphs show the results of optimization considering gross material consumption, while the right-side graphs display the outcomes of optimization considering only net consumption.

Fig. 12 illustrates the Pareto fronts for optimizing the structure under a nodal overload of 50 kN, considering a single design variable. The blue solid line represents the objective of minimizing gross material consumption, while the orange dashed line represents the objective of minimizing net material consumption.

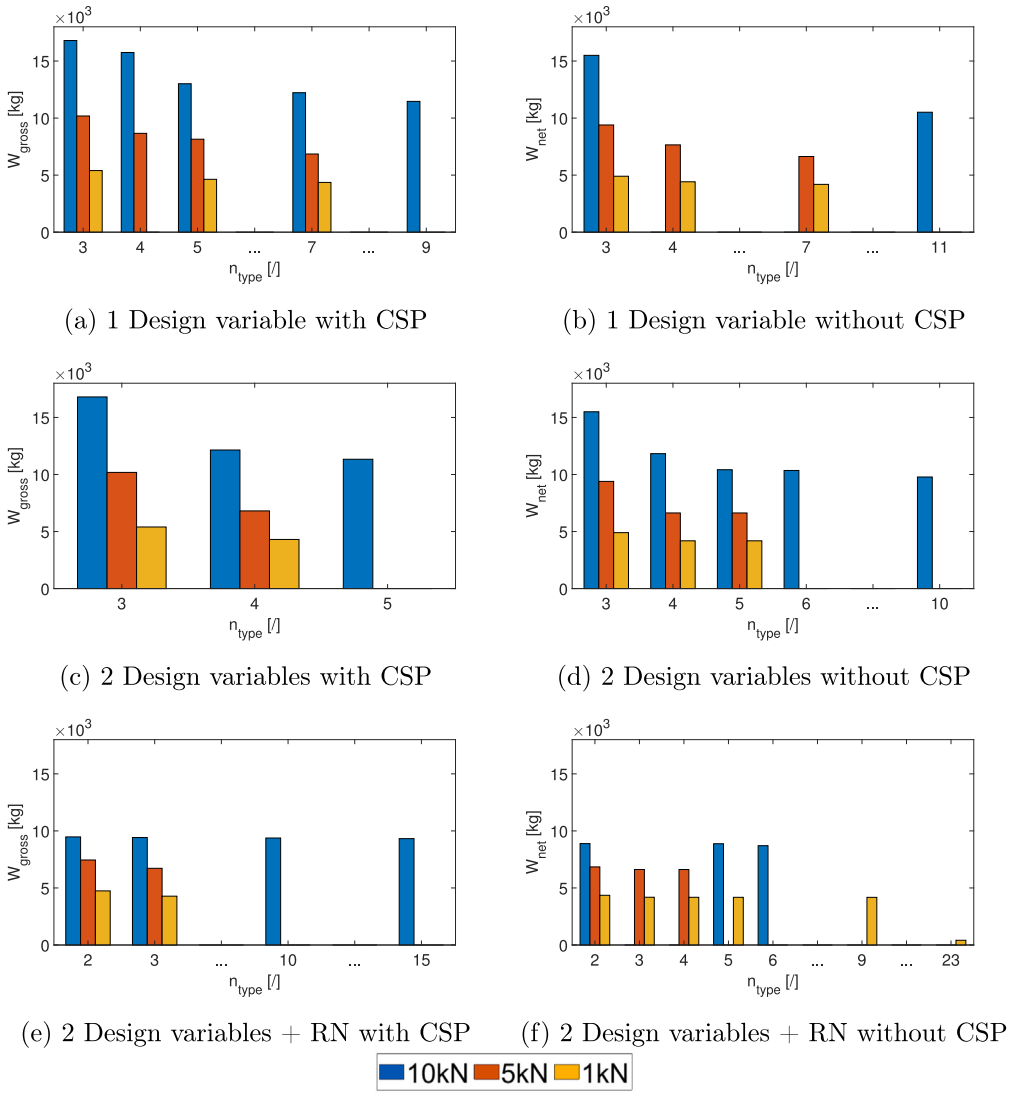

Fig. 11. Complex but regular gridshell structure optimization results considering different numbers of design variables and the adoption of Repulsive Nodes MRA. The results are presented comparing the differences in minimizing net or gross material consumption.

In this case, material consumption, whether gross or net, declines linearly as the number of structural elements increases. The Pareto front functions are monotonically decreasing because the two objective functions are antagonistic.

Fig. 12 provides a graphical representation of the optimal solutions, offering insight into the trade-offs between net and gross material consumption. A key distinction between the represented configurations lies in the relationship between profile height and material consumption. Configurations with lower profiles experience higher compressive stresses, necessitating the use of thicker structural elements, which in turn increase material consumption. Conversely, higher-profile configurations allow for slenderer structural elements that experience lower compressive stresses, ultimately reducing material usage.

4.3. Multiobjective optimization of free-form base gridshell structure

In the final example, a case involving free-form base geometry is presented to evaluate the proposed approach in a general scenario. The structure is defined by a free-form curve that outlines the base plan. The area enclosed by this curve is then discretized into a quadrangular mesh. Due to the irregularity of the base plan, the dimensions of the mesh elements vary, aiming for an average edge length of 1.50 m. The mesh elements range from a minimum length of 0.80 m to a maximum length of 2.30 m. The basic mesh used in this example is illustrated in Fig. 13.

The final structural configuration obtained in this example (Fig. 14) is the most complex among those documented. Therefore, the optimization was conducted using up to three design variables. In the final analysis, the case where optimization considers the use of three different lengths, denoted as $L_{rope,i}$, combined with the Repulsive Nodes MRA, was also examined.

To facilitate comparison with previously reported cases, the analyses were conducted using the same load cases described earlier. Specifically, the self-weight of the structural elements was considered alongside four different nodal overloads: 1 kN, 5 kN, 10 kN, and 50 kN.

In this section, the results of the optimization process aimed at minimizing gross material consumption are presented. To determine

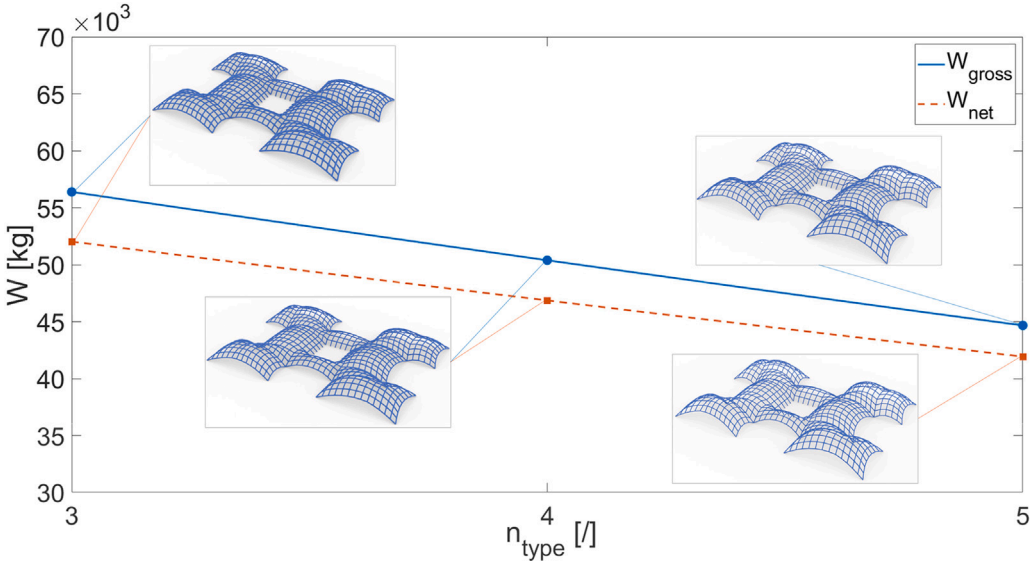

Fig. 12. Complex but regular gridshell structure optimization results considering a nodal overload of 50 kN and 1 design variable. Results represented as Pareto fronts in the objective functions search space.

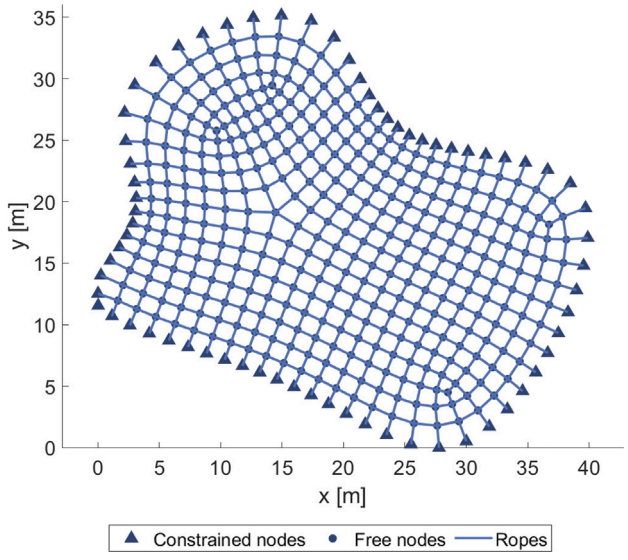

Fig. 13. Base mesh for the free-form gridshell structure.

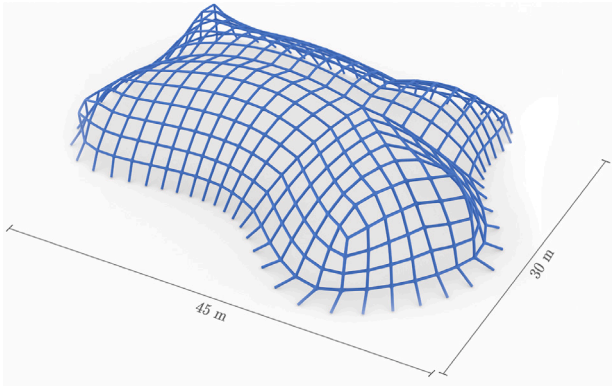

Fig. 14. Free-form base gridshell structure.

gross consumption, the minimum production waste was calculated using the CSP, as described in Section 3.3.1.

Table 2
Complex but regular gridshell optimization results in terms of use of material [kg] and construction complexity expressed as n_{type}.

	n_{type}	CSP: W_{gross}				No CSP: W_{net}			
		50 kN	10 kN	5 kN	1 kN	50 kN	10 kN	5 kN	1 kN
1 var	3	56 388	16 797	10 183	5399	52 029	15 498	9396	4903
	4	50 390	15 747	8662	\	46 865	\	7650	4416
	5	44 670	13 009	8149	4633	41 934	\	\	\
	7	\	12 224	6851	4361	\	\	6631	4189
	9	\	11 464	\	\	\	\	\	\
	11	\	\	\	\	\	10 513	\	\
2 var	3	56 388	16 797	10 183	5399	52 025	15 497	9395	4903
	4	44 112	12 147	6809	4307	41 924	11 826	6629	4188
	5	\	11 336	\	\	\	10 417	6628	4187
	6	\	\	\	\	\	10 353	\	\
	10	\	\	\	\	\	9781	\	\
2 var + RN	2	41 357	9474	7451	4743	38 750	8887	6845	4357
	3	41 120	9420	6723	4280	38 456	\	6618	4186
	4	\	\	\	\	38 162	\	6617	4182
	5	\	\	\	\	\	8875	\	4179
	6	\	\	\	\	38 154	8704	\	\
	7	\	\	\	\	38 146	\	\	\
	9	\	\	\	\	\	\	\	4177
	10	\	9377	\	\	\	\	\	\
	15	\	9322	\	\	\	\	\	\
	23	\	\	\	\	\	\	\	4159

The results of the optimization are presented in Figs. 15 and 16, which illustrate the Pareto fronts. Fig. 15 specifically shows the comparative outcomes of the optimization process for different nodal overloads as the number of design variables in the problem varies.

In each graph in Fig. 15, the number of design variables is held constant, and the resulting curves for increasing overloads are compared. It can be observed that the Pareto fronts become increasingly compressed and linear as the applied nodal loads decreases. The curves in the graphs exhibit the typical shape of a Pareto front for conflicting objective functions.

Furthermore, the graphs indicate that as the applied load decreases, the amount of structural material required also decreases. While this is an expected result, it confirms the accuracy of the analyses performed.

Fig. 16 presents the results, keeping the nodal overload constant for each graph and comparing the curves for varying numbers of design variables in the optimization problem. The graphs clearly show that as

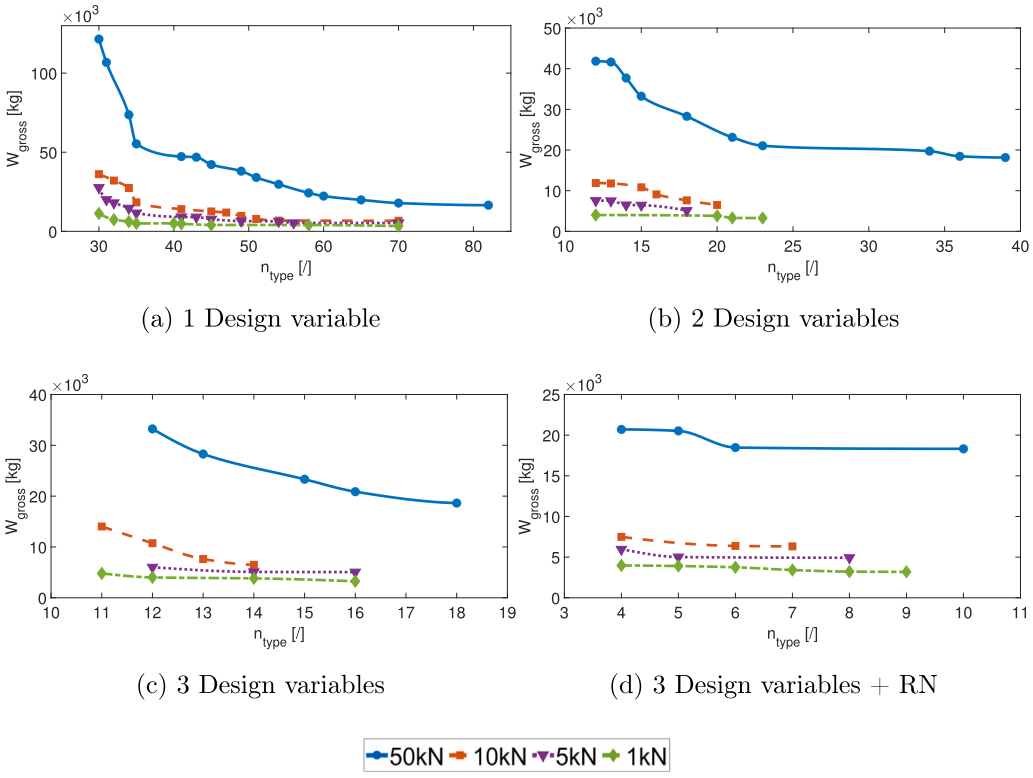

Fig. 15. Free-form base gridshell structure optimization results considering different numbers of design variables and the adoption of Repulsive Nodes MRA.

the number of design variables increases, both the amount of structural material and the number of structural element typologies decrease. This outcome is expected since the design variables represent the degrees of freedom in the optimization problem. More degrees of freedom allow for the exploration of new solutions, leading to higher-quality outcomes. Therefore, solutions with more design variables tend to be superior or at least equivalent to those related to the problem defined with fewer design variables.

Additionally, the graphs reveal a significant improvement when the number of design variables increases from one to two. However, when increasing the number from two to three, the distance between the Pareto fronts diminishes. This indicates that three design variables are sufficient to explore a comprehensive set of optimal solutions. Beyond this point, further increasing the degrees of freedom will not yield a significant improvement in the solutions.

In contrast, utilizing the Repulsive Nodes MRA significantly improves the results. This is evidenced by the greater distance between the Pareto fronts for the problem with three design variables using RN-MRA compared to the distance between the fronts for solutions with two or three design variables without RN-MRA.

This illustrates the effectiveness of employing the i-MRA techniques in identifying solutions that are simultaneously optimal in terms of structure and straightforward to be constructed.

Fig. 17 compares the Pareto fronts obtained for a nodal overload of 50 kN with a single design variable. This comparison focuses on solutions that minimize either gross structural material or net structural material. As before, the computation of minimum production deviations was performed using CSP. Additionally, Fig. 17 includes a visualization of the optimal structural shapes along the Pareto fronts. In this way it is possible to highlight the differences among the solutions in the Pareto set. It can be observed that the solutions obtained through the consideration and non-consideration of waste exhibit a high degree of visual similarity. This visualization aids the designer in selecting the optimal solution that best fits the specific project, taking into account both functional and aesthetic considerations. Even in this case, it can be observed that solutions with a lower number of structural element typologies are characterized by shallower geometries and thicker structural elements, resulting in higher material consumption. Conversely, solutions with lower material consumption feature less shallow gridshells with more slender structural elements, optimizing material usage with respect to ease of construction.

It should be noted that while the presented methodology provides optimized solutions for gridshell structures based on automatically generated meshes, further refinements to the base grid topology could potentially enhance the structural performance beyond what is achieved through parameter optimization alone. However, such topology optimization represents a separate design challenge beyond the scope of this work, which focuses on establishing a framework for parameter-based optimization of gridshell structures using predefined mesh topologies. The proposed methodology thus serves as an effective preliminary design tool that can be supplemented with targeted topological adjustments.

In this study, several simplifying assumptions were made to keep computations manageable during the conceptual design phase. First, beams were classified only by axis length, which does not fully reflect real-world geometric complexity. This approach overlooks factors such as bounding box dimensions, node normals, connection details, and fabrication tolerances. Moreover, the method assumes a single cross-section for all structural elements, whereas engineering practice typically employs different cross-sections to optimize material distribution [70]. Additionally, the focus on quadrangular gridshells, although beneficial from a manufacturing standpoint, does not reflect the higher performance often associated with alternative topologies [56,71]. Finally, facet planarity, a crucial metric that affects fabrication cost and environmental impact due to the challenges of forming non-planar or developable envelope materials [72,73]. has not been explicitly integrated into the optimization process. These limitations highlight areas for further refinement to better align the methodology with practical construction requirements.

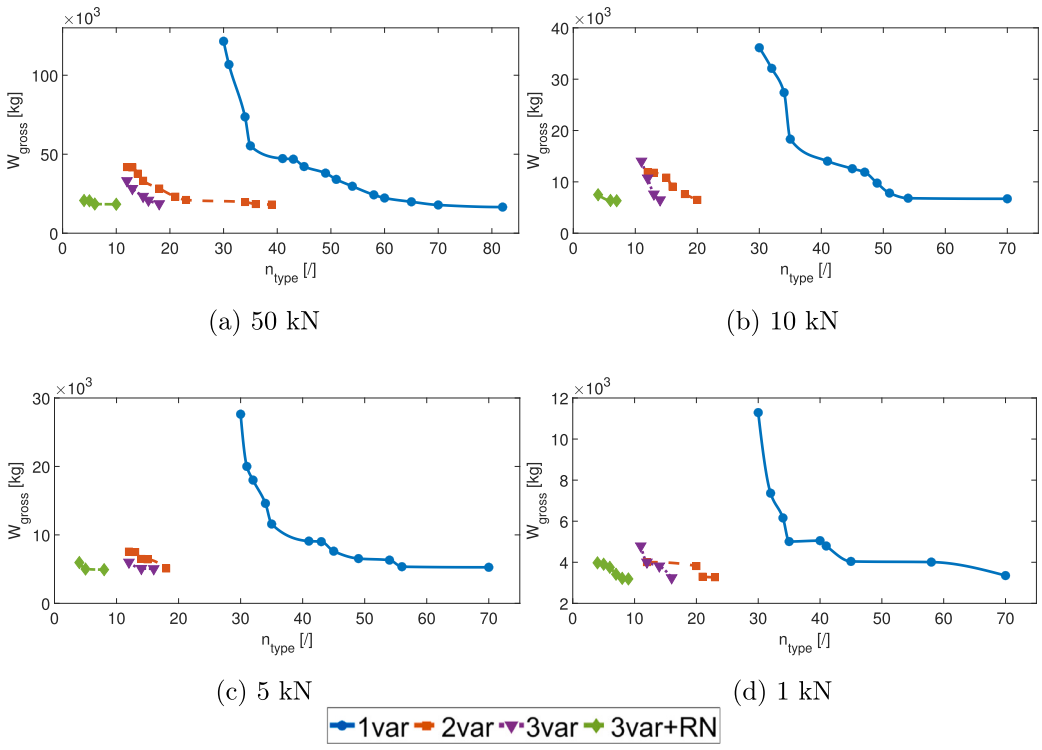

Fig. 16. Free-form base gridshell structure optimization results considering different nodal overloads.

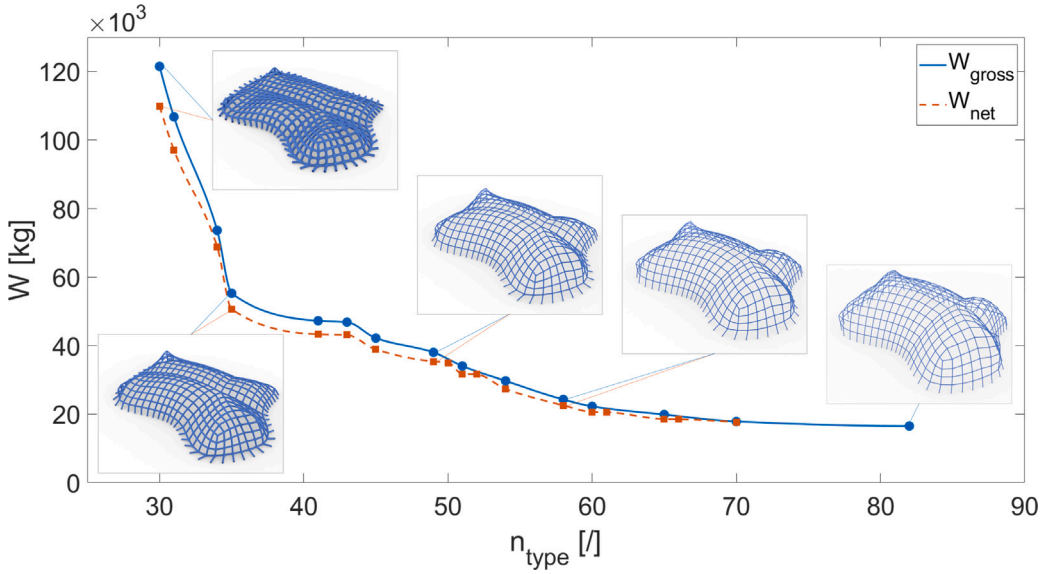

Fig. 17. Free-form base gridshell structure optimization results considering a nodal overload of 50 kN and 1 design variable. Results represented as Pareto fronts in the objective functions search space.

5. Conclusions and future developments

This paper introduced an advanced methodology for the preliminary design of gridshell structures, incorporating both form-finding and structural optimization to enhance structural efficiency, constructability and waste reduction.

The proposed approach combines the improved Multibody Rope Approach (i-MRA) with multi-objective metaheuristic optimization algorithms, specifically the Non-Dominated Sorting Genetic Algorithm II (NSGA II). By leveraging these techniques, the study aimed to optimize structural forms for minimal material usage and reduced construction complexity while also accounting for the production of waste.

The presented optimization process notably reduced the material required for constructing gridshell structures, leading to lower net and gross material consumption. This achievement is essential for mitigating the environmental and economic costs.

Furthermore, integrating waste management into the design process proved valuable. By addressing cutting patterns for structural elements,

the approach effectively reduced material waste, promoting more sustainable construction practices through a linear programming solution to the Cutting Stock Problem (CSP).

Additionally, the methodology streamlined the construction process by minimizing the variety of structural elements and optimizing their arrangement. This reduction in complexity not only facilitates a more efficient construction process but also potentially lowers costs and enhances the feasibility of realizing gridshell structures.

Lastly, the methodology demonstrated considerable versatility across various case studies. It adapted well to different design scenarios, from standard gridshells to more free-form gridshells, providing optimized solutions that met specific project requirements.

Overall, this paper underscores the potential of combining advanced form-finding techniques with structural optimization to drive sustainable innovations in the construction industry. The approach not only contributes to reducing the costs and the environmental footprint of gridshell structures but also offers practical solutions for the efficient realization of complex architectural designs.

Building upon the foundations of the present work, several promising avenues for future research have been identified. Future studies could incorporate a more comprehensive nesting analysis that considers not only the axis length but also the complete bounding box dimensions of beams, taking into account node normals and connection details. Although the current method allows the use of different cross-sections, it was deliberately simplified by assuming a single cross-section to reduce computational cost during extensive parametric analyses. In practical applications, where only one optimization run might be required, the method can be readily extended to accommodate multiple cross-sectional types. Furthermore, the integration of facet planarity constraints and panel nesting strategies would enhance material efficiency and reduce production waste.

CRediT authorship contribution statement

Jonathan Melchiorre: Writing – original draft, Visualization, Validation, Software, Methodology, Investigation, Formal analysis, Conceptualization. **Amedeo Manuello Bertetto:** Writing – review & editing, Methodology, Supervision, Project administration, Conceptualization. **Sigrid Adriaenssens:** Writing – review & editing, Visualization, Supervision. **Giuseppe Carlo Marano:** Writing – review & editing, Supervision, Project administration.

Declaration of competing interest

The authors declare that they have no known competing financial interests or personal relationships that could have appeared to influence the work reported in this paper.

Acknowledgements

Jonathan Melchiorre and Giuseppe Carlo Marano acknowledge the support of the project NODES which has received funding from the MUR – M4C2 1.5 of PNRR funded by the European Union - NextGenerationEU (Grant agreement no. ECS00000036). Amedeo Manuello Bertetto acknowledges the support of the Space It Up project funded by the Italian Space Agency, ASI, and the Ministry of University and Research, MUR, under contract n. 2024-5-E.0 - CUP n. I53D24000060005.

Data availability

No data was used for the research described in the article.

References

[1] J. Min, G. Yan, A.M. Abed, S. Elattar, M. Amine Khadimallah, A. Jan, H. Elhosiny Ali, The effect of carbon dioxide emissions on the building energy efficiency, Fuel 326 (2022) 124842, http://dx.doi.org/10.1016/j.fuel.2022.124842, URL https://www.sciencedirect.com/science/article/pii/S0016236122016854.

[2] M.M. Klufallah, M.F. Nuruddin, M.F. Khamidi, N. Jamaludin, Assessment of carbon emission reduction for buildings projects in Malaysia-A comparative analysis, in: E3S Web of Conferences, Vol. 3, EDP Sciences, 2014, p. 01016, http://dx.doi.org/10.1051/e3sconf/20140301016.

[3] O. Ortiz, F. Castells, G. Sonnemann, Sustainability in the construction industry: A review of recent developments based on LCA, Constr. Build. Mater. 23 (1) (2009) 28–39, http://dx.doi.org/10.1016/j.conbuildmat.2007.11.012, URL https://www.sciencedirect.com/science/article/pii/S0950061807003005.

[4] N.D. Lagaros, The environmental and economic impact of structural optimization, Struct. Multidiscip. Optim. 58 (4) (2018) 1751–1768, http://dx.doi.org/10.1007/s00158-018-1998-z.

[5] European Commission, European commission: Internal market, industry, entrepreneurship and SMEs, 2024, URL https://single-market-economy.ec.europa.eu/sectors/construction_en, (Accessed 15 April 2024).

[6] G.C. Marano, M.M. Rosso, J. Melchiorre, Optimization as a tool for seismic protection of structures*, in: G.P. Cimellaro (Ed.), Seismic Isolation, Energy Dissipation and Active Vibration Control of Structures, Springer International Publishing, Cham, 2023, pp. 100–113, http://dx.doi.org/10.1007/978-3-031-21187-4_8.

[7] S.H. Dyvik, B. Manum, A. Rønnquist, Gridshells in recent research—A systematic mapping study, Appl. Sci. 11 (24) (2021) http://dx.doi.org/10.3390/app112411731, URL https://www.mdpi.com/2076-3417/11/24/11731.

[8] H. Seifi, A. Rezaee Javan, S. Xu, Y. Zhao, Y.M. Xie, Design optimization and additive manufacturing of nodes in gridshell structures, Eng. Struct. 160 (2018) 161–170, http://dx.doi.org/10.1016/j.engstruct.2018.01.036, URL https://www.sciencedirect.com/science/article/pii/S0141029617320564.

[9] H. Wang, Z. Chen, G. Wen, G. Ji, Y. Min Xie, A robust node-shifting method for shape optimization of irregular gridshell structures, 34 (2021) 666–677, http://dx.doi.org/10.1016/j.istruc.2021.08.003, URL https://www.sciencedirect.com/science/article/pii/S2352012421007128.

[10] W. Zuo, M.-T. Chen, Y. Chen, O. Zhao, B. Cheng, J. Zhao, Additive manufacturing oriented parametric topology optimization design and numerical analysis of steel joints in gridshell structures, Thin-Walled Struct. 188 (2023) 110817, http://dx.doi.org/10.1016/j.tws.2023.110817, URL https://www.sciencedirect.com/science/article/pii/S0263823123002951.

[11] V. Tomei, D. Faiella, F. Cascone, E. Mele, Structural grammar for design optimization of grid shell structures and diagrid tall buildings, Autom. Constr. 143 (2022) 104588, http://dx.doi.org/10.1016/j.autcon.2022.104588, URL https://www.sciencedirect.com/science/article/pii/S0926580522004587.

[12] R. Mesnil, C. Douthe, O. Baverel, Non-standard patterns for gridshell structures: fabrication and structural optimization, J. Int. Assoc. Shell Spat. Struct. 58 (4) (2017) 277–286, http://dx.doi.org/10.20898/j.iass.2017.194.893.

[13] J.N. Richardson, S. Adriaenssens, R.F. Coelho, P. Bouillard, Discrete topology optimization: Connectivity for gridshells, in: Shell Structures for Architecture, Routledge, 2014, pp. 171–180, http://dx.doi.org/10.4324/9781315849270.

[14] C. Douthe, R. Mesnil, H. Orts, O. Baverel, Isoradial meshes: Covering elastic gridshells with planar facets, Autom. Constr. 83 (2017) 222–236, http://dx.doi.org/10.1016/j.autcon.2017.08.015, URL https://www.sciencedirect.com/science/article/pii/S0926580517307367.

[15] N. Montagne, C. Douthe, X. Tellier, C. Fivet, O. Baverel, Discrete Voss surfaces: Designing geodesic gridshells with planar cladding panels, Autom. Constr. 140 (2022) 104200, http://dx.doi.org/10.1016/j.autcon.2022.104200, URL https://www.sciencedirect.com/science/article/pii/S0926580522000735.

[16] R. Harris, J. Romer, O. Kelly, S. Johnson, Design and construction of the downland gridshell, Build. Res. Inf. 31 (6) (2003) 427–454, http://dx.doi.org/10.1080/0961321032000088007.

[17] E.L. Hernández, O. Baverel, C. Gengnagel, On the design and construction of elastic gridshells with irregular meshes, Int. J. Space Struct. 28 (3–4) (2013) 161–174, http://dx.doi.org/10.1260/0266-3511.28.3-4.161.

[18] M. Kilian, D. Pellis, J. Wallner, H. Pottmann, Material-minimizing forms and structures, ACM Trans. Graph. 36 (6) (2017) http://dx.doi.org/10.1145/3130800.3130827.

[19] C. Tang, X. Sun, A. Gomes, J. Wallner, H. Pottmann, Form-finding with polyhedral meshes made simple, ACM Trans. Graph. 33 (4) (2014) http://dx.doi.org/10.1145/2601097.2601213.

[20] R.A. Polyak, Regularized Newton method for unconstrained convex optimization, Math. Program. 120 (1) (2009) 125–145, http://dx.doi.org/10.1007/s10107-007-0143-3.

[21] J.J. Moré, The Levenberg-Marquardt algorithm: Implementation and theory, in: G.A. Watson (Ed.), Numerical Analysis, Springer Berlin Heidelberg, Berlin, Heidelberg, 1978, pp. 105–116, http://dx.doi.org/10.1007/BFb0067700.

[22] J. Chilton, C.-C. Chuang, Rooted in nature: aesthetics, geometry and structure in the shells of Heinz Isler, Nexus Netw. J. 19 (3) (2017) 763–785, http://dx.doi.org/10.1007/s00004-017-0357-5.

[23] L. Gründig, E. Moncrieff, P. Singer, D. Ströbel, A history of the principal developments and applications of the force density method in Germany 1970–1999, in: Proceedings of IASS-IACM 2000 Fourth International Colloquium on Computation of Shell & Spatial Structures, Chania-Crete, Greece, 2000, URL https://www.technet-gmbh.com/fileadmin/user_upload/technet/Publikationen/Easy/Density2.pdf.

[24] F. Marmo, L. Rosati, Reformulation and extension of the thrust network analysis, Comput. Struct. 182 (2017) 104–118, http://dx.doi.org/10.1016/j.compstruc.2016.11.016, URL https://www.sciencedirect.com/science/article/pii/S0045794916305697.

[25] H.-J. Schek, The force density method for form finding and computation of general networks, Comput. Methods Appl. Mech. Engrg. 3 (1) (1974) 115–134, http://dx.doi.org/10.1016/0045-7825(74)90045-0, URL https://www.sciencedirect.com/science/article/pii/0045782574900450.

[26] A. Kilian, J. Ochsendorf, Particle-spring systems for structural form finding, J. Int. Assoc. Shell Spat. Struct. 46 (2) (2005) 77–84, URL https://www.ingentaconnect.com/content/iass/jiass/2005/00000046/00000002/art00003.

[27] J.R.H. Otter, A.C. Cassell, R.E. Hobbs, Dynamic relaxation, Proc. Inst. Civ. Eng. 35 (4) (1966) 633–656, http://dx.doi.org/10.1680/iicep.1966.8604.

[28] M.R. Barnes, S. Adriaenssens, M. Krupka, A novel torsion/bending element for dynamic relaxation modeling, Comput. Struct. 119 (2013) 60–67, http://dx.doi.org/10.1016/j.compstruc.2012.12.027, URL https://www.sciencedirect.com/science/article/pii/S0045794913000072.

[29] A. Manuello, Multi-body rope approach for grid shells: Form-finding and imperfection sensitivity, Eng. Struct. 221 (2020) 111029, http://dx.doi.org/10.1016/j.engstruct.2020.111029, URL https://www.sciencedirect.com/science/article/pii/S0141029620309895.

[30] I.M. Rian, M. Sassone, S. Asayama, From fractal geometry to architecture: Designing a grid-shell-like structure using the Takagi–Landsberg surface, Comput.-Aided Des. 98 (2018) 40–53, http://dx.doi.org/10.1016/j.cad.2018.01.004, URL https://www.sciencedirect.com/science/article/pii/S0010448518300423.

[31] Z. Zhao, D. Yu, T. Zhang, N. Zhang, H. Liu, B. Liang, L. Xian, Efficient form-finding algorithm for freeform grid structures based on inverse hanging method, J. Build. Eng. 46 (2022) 103746, http://dx.doi.org/10.1016/j.jobe.2021.103746, URL https://www.sciencedirect.com/science/article/pii/S2352710221016041.

[32] W. Huang, C. Wu, J. Hu, W. Gao, Weaving structure: A bending-active gridshell for freeform fabrication, Autom. Constr. 136 (2022) 104184, http://dx.doi.org/10.1016/j.autcon.2022.104184, URL https://www.sciencedirect.com/science/article/pii/S0926580522000577.

[33] C. Chianese, L. Rosati, F. Marmo, Isogeometric form finding of membrane shells by optimised airy stress function, Comput. Methods Appl. Mech. Engrg. 426 (2024) 116946, http://dx.doi.org/10.1016/j.cma.2024.116946, URL https://www.sciencedirect.com/science/article/pii/S0045782524002020.

[34] M. Bagneris, R. Motro, B. Maurin, N. Pauli, Structural morphology issues in conceptual design of double curved systems, Int. J. Space Struct. 23 (2) (2008) 79–87, http://dx.doi.org/10.1260/026635108785260560.

[35] K. Yamamoto, T. Ogawa, M. Fujimoto, C. Lazaro, T. Takeuchi, S.-D. Xue, P.-S. Chen, S. Kato, State-of-the-art for optimization of forms and strength for reticulated shells, in: International Association for Shell and Spatial Structures 2012: from Spatial Structures To Space Structures, 2012, URL https://www.researchgate.net/publication/266078483_State-of-the-Art_for_Optimization_of_Forms_and_Strength_for_Reticulated_Shells.

[36] S. Adriaenssens, P. Block, D. Veenendaal, C. Williams, Shell Structures for Architecture: Form Finding and Optimization, Routledge, ISBN: 9780415840606, 2014, http://dx.doi.org/10.4324/9781315849270.

[37] L. Bouhaya, O. Baverel, J.-F. Caron, Optimization of gridshell bar orientation using a simplified genetic approach, Struct. Multidiscip. Optim. 50 (2014) 839–848, http://dx.doi.org/10.1007/s00158-014-1088-9.

[38] J.N. Richardson, S. Adriaenssens, R. Filomeno Coelho, P. Bouillard, Coupled form-finding and grid optimization approach for single layer grid shells, Eng. Struct. 52 (2013) 230–239, http://dx.doi.org/10.1016/j.engstruct.2013.02.017, URL https://www.sciencedirect.com/science/article/pii/S0141029613000813.

[39] E. Grande, M. Imbimbo, V. Tomei, Structural optimization of grid shells: Design parameters and combined strategies, J. Archit. Eng. 24 (1) (2018) 04017027, http://dx.doi.org/10.1061/(ASCE)AE.1943-5568.0000286, URL https://ascelibrary.org/doi/abs/10.1061/%28ASCE%29AE.1943-5568.0000286.

[40] J. Rombouts, G. Lombaert, L. De Laet, M. Schevenels, A novel shape optimization approach for strained gridshells: Design and construction of a simply supported gridshell, Eng. Struct. 192 (2019) 166–180, http://dx.doi.org/10.1016/j.engstruct.2019.04.101, URL https://www.sciencedirect.com/science/article/pii/S0141029618336071.

[41] A. Manuello Bertetto, J. Melchiorre, G.C. Marano, Improved multi-body rope approach for free-form grid shells, in: S. Gabriele, A. Manuello Bertetto, F. Marmo, A. Micheletti (Eds.), Shell and Spatial Structures, Springer Nature Switzerland, Cham, 2024, pp. 231–240, http://dx.doi.org/10.1007/978-3-031-44328-2_24.

[42] K. Deb, Multi-objective optimisation using evolutionary algorithms: An introduction, in: L. Wang, A.H.C. Ng, K. Deb (Eds.), Multi-Objective Evolutionary Optimisation for Product Design and Manufacturing, Springer London, London, 2011, pp. 3–34, http://dx.doi.org/10.1007/978-0-85729-652-8_1.

[43] A.M. Bertetto, J. Melchiorre, G.C. Marano, Improved multi-body rope approach for free-form gridshell structures using equal-length element strategy, Autom. Constr. 161 (2024) 105340, http://dx.doi.org/10.1016/j.autcon.2024.105340, URL https://www.sciencedirect.com/science/article/pii/S0926580524000761.

[44] R. McNeel, et al., Rhinoceros 3D, Version 7.0, Robert McNeel & Associates, Seattle, WA, 2023, URL https://www.rhino3d.com/.

[45] K. Deb, A. Pratap, S. Agarwal, T. Meyarivan, A fast and elitist multiobjective genetic algorithm: NSGA-II, IEEE Trans. Evol. Comput. 6 (2) (2002) 182–197, http://dx.doi.org/10.1109/4235.996017.

[46] J.G. Hobbie, A.H. Gandomi, I. Rahimi, A comparison of constraint handling techniques on NSGA-II, Arch. Comput. Methods Eng. 28 (5) (2021) 3475–3490, http://dx.doi.org/10.1007/s11831-020-09525-y.

[47] A.C. Cherri, M.N. Arenales, H.H. Yanasse, K.C. Poldi, A.C. Gonçalves Vianna, The one-dimensional cutting stock problem with usable leftovers – A survey, European J. Oper. Res. 236 (2) (2014) 395–402, http://dx.doi.org/10.1016/j.ejor.2013.11.026, URL https://www.sciencedirect.com/science/article/pii/S0377221713009430.

[48] L.R. Ford, D.R. Fulkerson, A suggested computation for maximal multi-commodity network flows, Manag. Sci. 5 (1) (1958) 97–101, http://dx.doi.org/10.1287/mnsc.5.1.97.

[49] P.C. Gilmore, R.E. Gomory, A linear programming approach to the cutting-stock problem, Oper. Res. 9 (6) (1961) 849–859, http://dx.doi.org/10.1287/opre.9.6.849.

[50] C. Cheng, B. Feiring, T. Cheng, The cutting stock problem — a survey, Int. J. Prod. Econ. 36 (3) (1994) 291–305, http://dx.doi.org/10.1016/0925-5273(94)00045-X, URL https://www.sciencedirect.com/science/article/pii/092552739400045X.

[51] MATLAB, Version (R2022b) Access (8 November 2023), The MathWorks Inc., Natick, Massachusetts, 2022, URL https://www.mathworks.com/products/matlab.html.

[52] D. Veenendaal, P. Block, An overview and comparison of structural form finding methods for general networks, Int. J. Solids Struct. 49 (26) (2012) 3741–3753, http://dx.doi.org/10.1016/j.ijsolstr.2012.08.008, URL https://www.sciencedirect.com/science/article/pii/S002076831200337X.

[53] C.A.C. Coello, Evolutionary Algorithms for Solving Multi-Objective Problems, Springer, 2007, http://dx.doi.org/10.1007/978-0-387-36797-2.

[54] M. Paradiso, F. Marmo, L. Rosati, Consistent derivation of a beam model from the saint Venant's solid model, Int. J. Solids Struct. 159 (2019) 90–110, http://dx.doi.org/10.1016/j.ijsolstr.2018.09.021, URL https://www.sciencedirect.com/science/article/pii/S0020768318303779.

[55] M. Paradiso, S. Sessa, N. Vaiana, F. Marmo, L. Rosati, Shear properties of isotropic and homogeneous beam-like solids having arbitrary cross sections, Int. J. Solids Struct. 216 (2021) 231–249, http://dx.doi.org/10.1016/j.ijsolstr.2021.01.012, URL https://www.sciencedirect.com/science/article/pii/S0020768321000202.

[56] S. Malek, T. Wierzbicki, J. Ochsendorf, Buckling of spherical cap gridshells: A numerical and analytical study revisiting the concept of the equivalent continuum, Eng. Struct. 75 (2014) 288–298, http://dx.doi.org/10.1016/j.engstruct.2014.05.049, URL https://www.sciencedirect.com/science/article/pii/S0141029614003472.

[57] J. Melchiorre, F. Bazzucchi, A. Manuello Bertetto, G.C. Marano, Postbuckling echoes of iMRA introduced variation in gridshells mechanical behaviour, in: S. Gabriele, A. Manuello Bertetto, F. Marmo, A. Micheletti (Eds.), Shell and Spatial Structures, Springer Nature Switzerland, Cham, 2024, pp. 379–389, http://dx.doi.org/10.1007/978-3-031-44328-2_39.

[58] J. Melchiorre, A. Manuello Bertetto, S. Invernizzi, G.C. Marano, F. Bazzucchi, Dakar Mosque gridshell: Exploring the benefits of the improved multibody rope approach through postbuckling analysis, Struct. 61 (2024) 106059, http://dx.doi.org/10.1016/j.istruc.2024.106059, URL https://www.sciencedirect.com/science/article/pii/S235201242400211X.

[59] S. Kato, K. Abedi, P. Chen, F. Fan, M. Fujimoto, C. Gantes, K. Ishikawa, K. Kawaguchi, S.-D. Kim, C. Lázaro, Y. Luo, S. Nakazawa, T. Ogawa, T. Takeuchi, Y. Taniguichi, K. Tsavdaridis, S.-D. Xue, K. Yamamoto, Q. Zhang, l. Xuecong, Guide to buckling load evaluation of metal reticulated roof structures Wg08 V20180103, 2014, URL https://www.researchgate.net/publication/355159633_Guide_to_Buckling_Load_Evaluation_of_Metal_Reticulated_Roof_Structures_WG08_v20180103.

[60] F. Bazzucchi, A. Manuello, A. Carpinteri, Instability load evaluation of shallow imperfection-sensitive structures by form and interaction parameters, Eur. J. Mech. A Solids 66 (2017) 201–211, http://dx.doi.org/10.1016/j.euromechsol.2017.07.008, URL https://www.sciencedirect.com/science/article/pii/S099775381730253X.

[61] E.E.C. for Constructional Steelwork, Design of Steel Structures: Eurocode 3: Design of Steel Structures, Ernst & Sohn, Berlin, Germany, 2016, URL https://tragwerk-und-statik.de/dokument/Design_of_Steel_Structures_Eurocode_3_Design_of_Steel_Structures._Part_1-1_General_Rules_and_Rules_for_Buildings_1607358374_7558.pdf.

[62] L.V. Kantorovich, Mathematical methods of organizing and planning production, Manag. Sci. 6 (4) (1960) 366–422, http://dx.doi.org/10.1287/mnsc.6.4.366.

[63] P.C. Gilmore, R.E. Gomory, A linear programming approach to the cutting stock problem—Part II, Oper. Res. 11 (6) (1963) 863–888, http://dx.doi.org/10.1287/opre.11.6.863.

[64] Global Optimization Toolbox MATLAB, Function "Gamultiobj", The MathWorks Inc., Natick, Massachusetts, 2024, URL https://it.mathworks.com/help/gads/gamultiobj.html.

[65] K. Deb, S. Agrawal, A. Pratap, T. Meyarivan, A fast elitist non-dominated sorting genetic algorithm for multi-objective optimization: NSGA-II, in: M. Schoenauer, K. Deb, G. Rudolph, X. Yao, E. Lutton, J.J. Merelo, H.-P. Schwefel (Eds.), Parallel Problem Solving from Nature PPSN VI, Springer Berlin Heidelberg, Berlin, Heidelberg, 2000, pp. 849–858, http://dx.doi.org/10.1007/3-540-45356-3_83.

[66] N. Srinivas, K. Deb, Muiltiobjective optimization using nondominated sorting in genetic algorithms, Evol. Comput. 2 (3) (1994) 221–248, http://dx.doi.org/10.1162/evco.1994.2.3.221.

[67] B.L. Miller, D.E. Goldberg, Genetic algorithms, tournament selection, and the effects of noise, Complex Systems 9 (3) (1995) 193–212, URL https://wpmedia.wolfram.com/sites/13/2018/02/09-3-2.pdf.

[68] J. Yang, C.K. Soh, Structural optimization by genetic algorithms with tournament selection, J. Comput. Civ. Eng. 11 (3) (1997) 195–200, http://dx.doi.org/10.1061/(ASCE)0887-3801(1997)11:3(195).

[69] C.W. Ahn, R. Ramakrishna, Elitism-based compact genetic algorithms, IEEE Trans. Evol. Comput. 7 (4) (2003) 367–385, http://dx.doi.org/10.1109/TEVC.2003.814633.

[70] P.J. Knippers, T. Helbig, Recent developments in the design of glazed grid shells, Int. J. Space Struct. 24 (2) (2009) 111–126, http://dx.doi.org/10.1260/026635109789043205, arXiv:https://doi.org/10.1260/026635109789043205.

[71] R. Mesnil, C. Douthe, O. Baverel, B. Léger, Linear buckling of quadrangular and kagome gridshells: A comparative assessment, Eng. Struct. 132 (2017) 337–348, http://dx.doi.org/10.1016/j.engstruct.2016.11.039, URL https://www.sciencedirect.com/science/article/pii/S0141029616313141.

[72] J. Glymph, D. Shelden, C. Ceccato, J. Mussel, H. Schober, A parametric strategy for free-form glass structures using quadrilateral planar facets, Autom. Constr. 13 (2) (2004) 187–202, http://dx.doi.org/10.1016/j.autcon.2003.09.008, Conference of the Association for Computer Aided Design in Architecture. URL https://www.sciencedirect.com/science/article/pii/S0926580503001055.

[73] Y. Liu, H. Pottmann, J. Wallner, Y.-L. Yang, W. Wang, Geometric modeling with conical meshes and developable surfaces, in: ACM SIGGRAPH 2006 Papers, SIGGRAPH '06, Association for Computing Machinery, New York, NY, USA, 2006, pp. 681–689, http://dx.doi.org/10.1145/1179352.1141941.